PNL-4210
UC-60

The Wake of the MOD-OA1 Wind Turbine at Two Rotor Diameters Downwind on December 3, 1981

J. R. Connell
R. L. George

November 1982

Prepared for the U.S. Department of Energy
under Contract DE-AC06-76RLO 1830

Pacific Northwest Laboratory
Operated for the U.S. Department of Energy
by Battelle Memorial Institute

Battelle

PNL-4210

DISCLAIMER

PACIFIC NORTHWEST LABORATORY
operated by
BATTELLE
for the
UNITED STATES DEPARTMENT OF ENERGY
under Contract DE-AC06-76RLO 1830

Printed in the United States of America
Available from
National Technical Information Service
United States Department of Commerce
5285 Port Royal Road
Springfield, Virginia 22151

NTIS Price Codes
Microfiche A01

Printed Copy

Pages	Price Codes
001-025	A02
026-050	A03
051-075	A04
076-100	A05
101-125	A06
126-150	A07
151-175	A08
176-200	A09
201-225	A010
226-250	A011
251-275	A012
276-300	A013

PNL-4210
UC-60

THE WAKE OF THE MOD-0A1 WIND TURBINE AT TWO ROTOR DIAMETERS DOWNWIND ON DECEMBER 3, 1981

J. R. Connell
R. L. George

November 1982

Prepared for
the U.S. Department of Energy
under Contract DE-AC06-76RL0-1830

Pacific Northwest Laboratory
Richland, Washington 99352

SUMMARY

This report describes the characteristics of a wake of the MOD-0A1 wind turbine at Clayton, New Mexico. The single-case study is drawn from a group of wake cases measured with a set of 18 anemometers arranged in a vertical plane array (VPA) normal to the mean wind at a distance of two rotor diameters from the turbine.[a] In addition, references for a few mathematical models of wakes of turbines are cited along with several fluid laboratory simulations of turbine wakes as the main guides to the properties of full-scale wind turbine wakes. Two reports of wake measurements for small turbines in the atmosphere are found to have the most useful if meager information available for testing the simulations and models.

The terrain at the measurement site is quite uniform and has a roughness length, z_o, of about 2 cm. The measurements analyzed for this report were made on December 3, 1981 in a neutrally stable wind whose speed at hub height was about 10.7 ms^{-1}. The turbine operated at just below its rated power (200 kW). The wind speed, turbulence and wind direction were quite stationary during the 4.27 minute study period. The wind velocities were sampled at all anemometers on the array once every 0.25 second.

Several features of the wake at a distance of two rotor diameters from the turbine ($x/D = 2$) were studied. These features, as seen at the vertical plane orthogonal to the axis of the VPA (i.e., the nominal axis of the wake) were:

1. mean wind speed profiles;
2. turbulence intensity and integral length scale profiles;
3. spectra of turbulence at the fixed anemometer locations and the rotationally sampled spectrum as a second turbine in the wake of the first one would experience it;

(a) These measurements were a secondary (opposite-wind-direction) part of a larger program to correlate the wind at the VPA with the turbine response to the wind. Several more reports will follow this one to describe the MOD-0A1 wake under different wind speed and atmospheric static stability conditions.

4. inferred induction factor, rotor efficiency and power coefficient of the turbine;

5. the two-dimensional crosswind planar distribution of the wake wind speed;

6. the average axial rate of reenergizing of the wake from x/D = 0 to x/D = 2 and a comparison of the measured wake properties with those indicated by the simple models of Lissaman et al. (1982) and Eberle (1981).

The following properties of the wake were observed. Rotor blade vortices were well mixed into the wake turbulence and were not separately detectable at x/D = 2. Wake swirl about the along-wind axis had a value not greater than 0.025 rad s^{-1}. (Note: All wake characteristics described herein are for x/D = 2 unless otherwise stated.) The maximum axial wind speed deficit was $\Delta U/U_\infty = 0.25$.

The axial induction factor, a, calculated using measured winds and one-dimensional momentum theory had a value of a = 0.13 at $U_\infty = 10.7$ ms^{-1}. The NASA aerodynamic model of the MOD-OA1 gave a value of a = 0.13 for $U_\infty = 10$ ms^{-1}.

Extra turbulence energy existed in the edge of the wake at a frequency of about n = 0.025 Hz. This peak of extra turbulence energy existed throughout the wake but diminished toward the center. Spectral peaks at n = 0.25 Hz and 0.50 Hz, equivalent to wavelengths of λ = 1 D and 0.5 D, occurred particularly on the left side of the wake. The wake turbulence integrated over all frequencies was only slightly more energetic than the ambient turbulence. The time integral scale of turbulence in the wake was significantly larger than is expected for the ambient flow.

The cross-wake plane analyses of wind speeds revealed a nearly circular inner portion and a strongly elliptical outer portion. The major axis of the elliptical portion was horizontal. The ratio of the lengths of the major and minor axes was 1.6 based upon the shape of the velocity deficit line for $\Delta U/U_\infty = 0.01$.

An estimate of the average rate of reenergizing of the wake, using measurements of mean wind energy flow and turbine power, suggests that entrainment with ambient air was rapid. The average rate of reenergizing between the turbine and the vertical plane array at x/D = 2 was estimated to be about 700 kW per rotor diameter distance downstream. This is as much energy as flowed through the upstream projection of the rotor disc. If that average rate continued, the wake would have been substantially reenergized at a downwind distance of x/D = 5.5. At x/D = 2 the power ratio had a magnitude $P/P_{\infty} = 0.6$.

Some wake characteristics observed on December 3, 1981 were compared with the corresponding ones for several simple wake models (e.g., Lissaman et al. 1982 and Eberle 1981). The models include mixing of ambient air into a wake or an equivalent coaxial jet. The shapes of the vertical and horizontal profiles of mean wind speed are all very similar. However, the new measurements at x/D = 2 match up best with the Eberle model for $x/D \geq 5$. The rate of spread of the wake is in fair agreement with the models of far wake horizontal spread. Agreement for other properties from theoretical or fluid laboratory simulations was weaker.

Many of the comparisons between the MOD-0A1 wake measurements and the simple models of wakes are made in Table 1 (see Section 8).

It is concluded that the MOD-0A1 turbine wake entered into a far wake condition rapidly on December 3, 1981. The turbine was at near-rated power and was operating in a neutrally-layered atmospheric boundary layer. The microscale wind properties of the wake that would affect fatigue and power performance of a second MOD-0A turbine in the wake of the first one suggest that turbines might be successfully operated closer together than was previously thought to be efficient or safe.

Additional modeling and field measurements of wakes are required to substantially improve the understanding of turbine wakes. The complexity of wakes in the atmospheric boundary layer and the difficulty but possibility of measuring them has been demonstrated. Specializing wake models for use in turbine and turbine array design may require a few well chosen and well measured

wind properties of wakes for each distinctly different type of turbine and location. Accurate modeling of wake conditions in complex terrain will require great skill in measurement and analysis. However, these same complexities may mean that wakes will not be as much of a problem as has been previously thought for turbines downwind of other turbines in complex terrain.

ACKNOWLEDGMENTS

The authors thank especially the following reviewers for their comments on the first draft of this report: J. C. Barnard, DOE/PNL; J. C. Doran, DOE/PNL; A. C. Hansen, DOE/RF; P. Lissaman, Aerovironment, Inc.; and T. R. Richards, NASA/LeRC.

Thanks also to D. L. Atkin for skill and steadfastness in typing the drafts and the final manuscript and to E. L. Owczarski for editing service beyond the normal call of duty.

CONTENTS

FIGURES

FIGURES (Continued)

NOMENCLATURE

a	Axial induction factor
C_p	Power coefficient
D	Rotor diameter
E	Blade efficiency (Section 5), flux of kinetic energy (Section 7)
HAWT	Horizontal axis wind turbine
Hz	Hertz
n	Frequency of fluctuation of a sinusoidal component of the variation of any function of time decomposed by a Fourier analysis method
P	Rotation period, or the corresponding frequency, of a turbine rotor. Alternatively, the symbol for power.
P_∞	Power in the far upwind location of the disk of rotation
rad	radian
R	D/2
U	Directional component of wind parallel to the axis of the VPA
U_0	U at the axis of the wake at an arbitrary distance, x
U_∞	Free stream value of U at any specified height, or at the hub height of the turbine
V	Directional component of wind, perpendicular to U
VPA	Vertical plane array
W	1) Meteorological tower width, 2) vertical component of wind, (orthogonal to U and V)
x	Direction along the VPA-turbine axis
Y	Horizontal direction perpendicular to the turbine-VPA axis

z_o	Roughness length for the logarithmic expression for wind speed as a function of height
ΔU	Axial wind speed deficit at the axis of the wake at arbitrary distance from the turbine, $\Delta U = U_0 - U_\infty$
$\Delta U/U_\infty$	Nondimensional wake deficit
λ	Wavelength of a turbulent eddy (or wind speed fluctuation)
σ_u	Root-mean-square value of axial wind speed fluctuations

THE WAKE OF THE MOD-OA1 WIND TURBINE AT TWO ROTOR DIAMETERS DOWNWIND ON DECEMBER 3, 1981

J. R. Connell and R. L. George
Pacific Northwest Laboratory

1. INTRODUCTION AND BACKGROUND DISCUSSION

Utilization of wind turbines in arrays for wind farms, as well as some aspects of aerodynamic modeling and design of wind turbines, requires detailed knowledge about the characteristics of turbine wakes. Up to the present time the wind energy community has had the benefit of several mathematically stated models of the geometry of a horizontal-axis turbine wake in a simplified boundary layer (Lissaman 1979; Sforza et al. 1979; Wilson et al. 1976; Crafoord 1979; and Eberle 1981). In addition, wind tunnel modeling of single turbine wakes has provided insight into the distribution of mean wind speed and turbulence intensity throughout the wake (Builtjes 1979; Vermeulen 1978; Boschloo 1977; Blackwell and Sheldahl 1977; and others). The physical models of turbines have varied from a porous disk or grid to scaled-down rotor models. It is important for the present purpose only to note that there are limitations in all of the existing models related to scaling, modeling of the interaction between the wind and the turbine and modeling of the turbine layer of the atmosphere.

Several notable attempts to measure the properties of wakes of full-scale operating wind turbines have been made in what we will call field studies. Vertical profiles of 4-hour averages of 10-minute grab samples in the wake of a horizontal-axis wind turbine (HAWT) at Kalbregnen, Sweden, have been reported by Faxen (1978). The two-bladed turbine, with an 18 m blade diameter, was rated at 63 kW. Two 42-m meteorological towers were set at 5.6 diameters (about 100 m) from the turbine, one upwind and one downwind. Anemometers were placed on the towers at 7 m and at each increment of 7 m up to 42 m above the ground. There was no anemometer at hub height, z = 24 m. The terrain was

irregular and the towers were placed within 20 m of the edge of a dense forest. The resulting mean wind profiles are shown in Figure 1 for two wind speeds. The data do not collapse into a single case when normalized by mean wind speed or power density or power output of the turbine. The deficit is unsymmetric. Many factors of the field measurement design may be cited as increasing the uncertainty of the study, but it appears that a substantial maximum speed deficit ($\Delta U/U_\infty \doteq 0.1$ and 0.25 in the two cases shown) existed at 5.6 diameters (D) from the turbine.

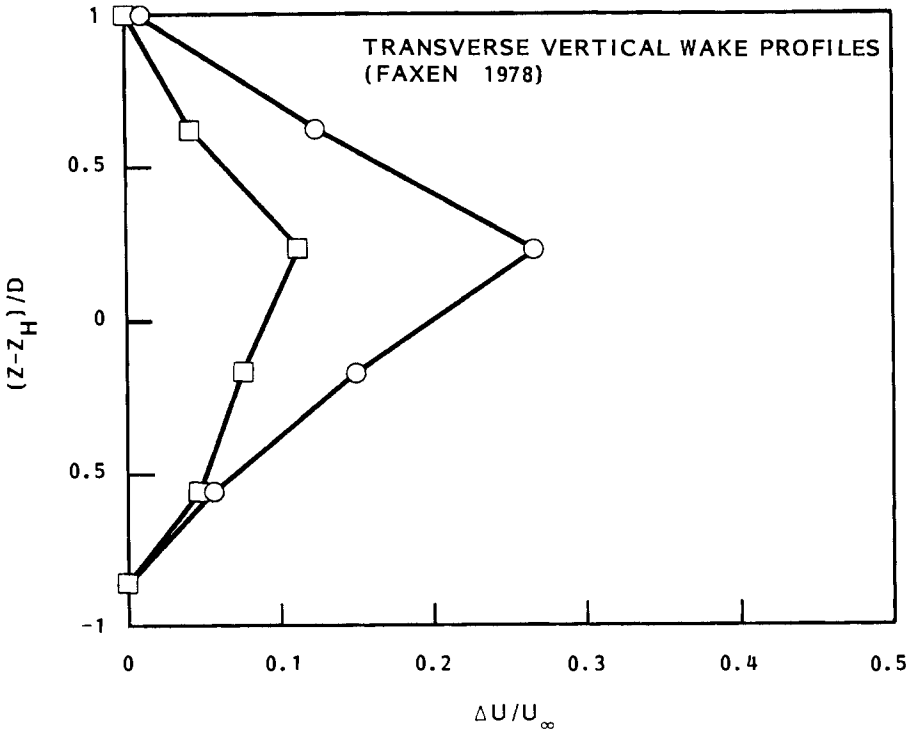

FIGURE 1. Nondimensional plot of vertical profiles of wind speed deficit at the nominal center plane of the wake of an 18-m diameter, 2-bladed HAWT at x/D = 5.5. Symbols: □ U_∞ = 6.9 ms^{-1}, P = 16 kW; ○ U_∞ = 8.2 ms^{-1}, P = 35 kW. (Adapted from Faxen 1978).

Vermeulen et al. (1979) studied the wake properties of a 5-m Darrieus turbine at distances downwind from 1.6 D to 7 D. Both mean wind and turbulence intensities were measured. Asymmetry and nonsteadiness of the wake were

observed. The far wake was reasonably well described. The wake deficit at x/D = 3 along the axis of the mean wake was about $(\Delta U/U_\infty) = 0.25$, which is about what Faxen observed at x/D = 5.6.

One additional field measurement program has successfully produced data about HAWT wakes and is considered here. Hansen (1980) at the Rocky Flats plant measured wakes of a three-bladed HAWT, with a 4-m blade diameter, in low-turbulence and negligible wind shear conditions. At x/D = 1.85 the wake deficit was on average about $\Delta U/U_\infty \doteqdot 0.7$ and at x/D = 5.1, $\Delta U/U_\infty \doteqdot 0.5$. The U_∞ was about 9 ms^{-1}, which corresponds to a peak value of C_p. The wake extended beyond 14 diameters downwind. The width of the wake was 2Y/D = 1.8 at x/D = 3 and 2Y/D = 2.8 at x/D = 11. The measurements were made with all systems moving through calm air using a railroad flatcar. The lateral profile was obtained by changing the location of the two anemometers between individual data runs and compositing all data onto one graph. The resulting profiles are somewhat irregular and unsymmetric and the data show considerable scatter. The data for x/D = 1.85 are reinterpreted in Figure 2, using the fact that the scattered data points have a sharply defined boundary. Wakes are not always steady. It is possible that the length of the potential core changed during the set of measurements that were composited. The wake deficit at x/D = 1.85 appeared to be in the range of $(U-U_\infty)/U_\infty = 0.6$ to 0.82.

Figure 3 shows the nondimensional wake deficit, $\Delta U/U_\infty$, as a function of free stream velocity, U_∞. There was no wind shear in Hansen's study. It is interesting to note that an apparent maximum wake deficit occurred at a value of $U_\infty = 7.3$ ms^{-1}. The magnitude of the maximum deficit is $\Delta U/U_\infty \doteqdot 2/3$. Thus $U_0/U_\infty = 1/3$ which is the value expected at the Betz limit condition on U_0 as shown for the actuator disc by Wilson et al. (1976). This leads one to suppose that proportionately more energy of the wake is in turbulence and swirl of the wake at $U_\infty = 7.3$ ms^{-1} than at $U_\infty = 9.1$ ms^{-1}, which corresponds to the maximum C_p of the turbine.

It is tempting to consider the impact of the balance between efficiency of the turbine in extraction of wind energy and the rate of recovery of wake

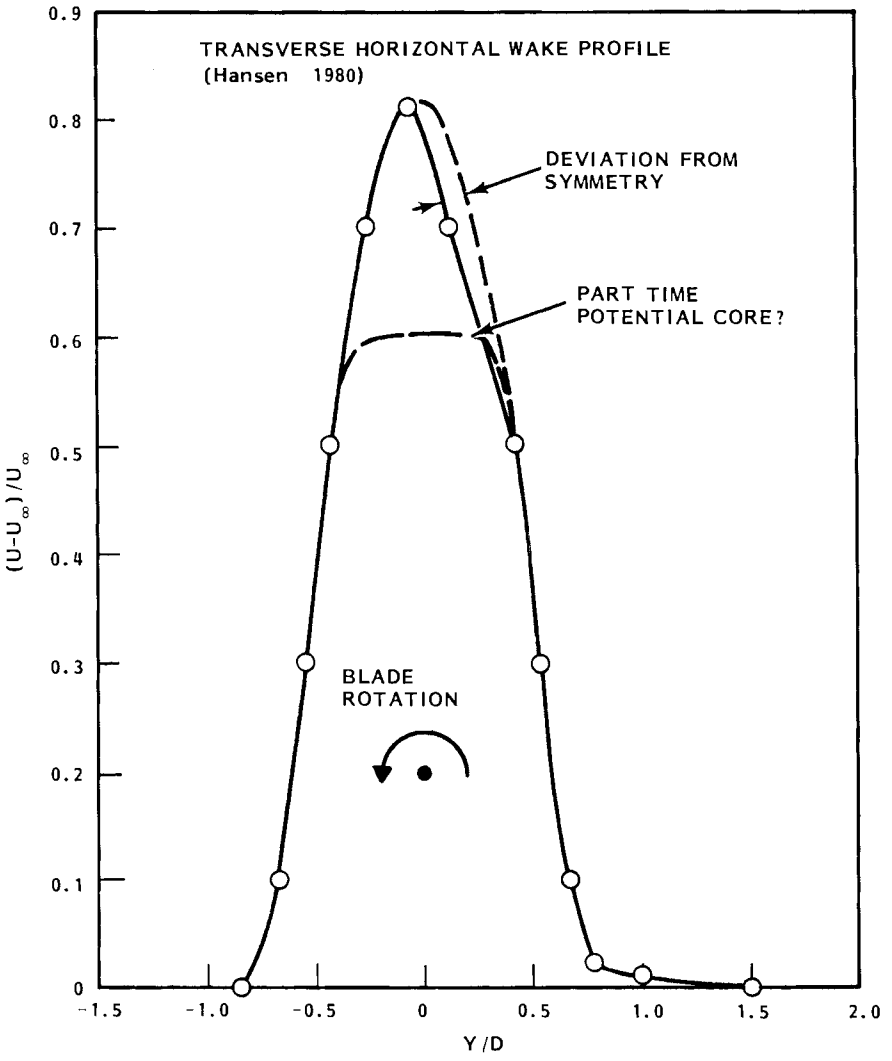

FIGURE 2. Nondimensional plot of horizontal cross-wake profile wind speed deficit at the nominal horizontal center plane of a 4-m diameter, 3-bladed HAWT at x/D = 1.85, U_∞ = 9.1 ms^{-1}. (Adapted from Hansen 1980, Figure 10).

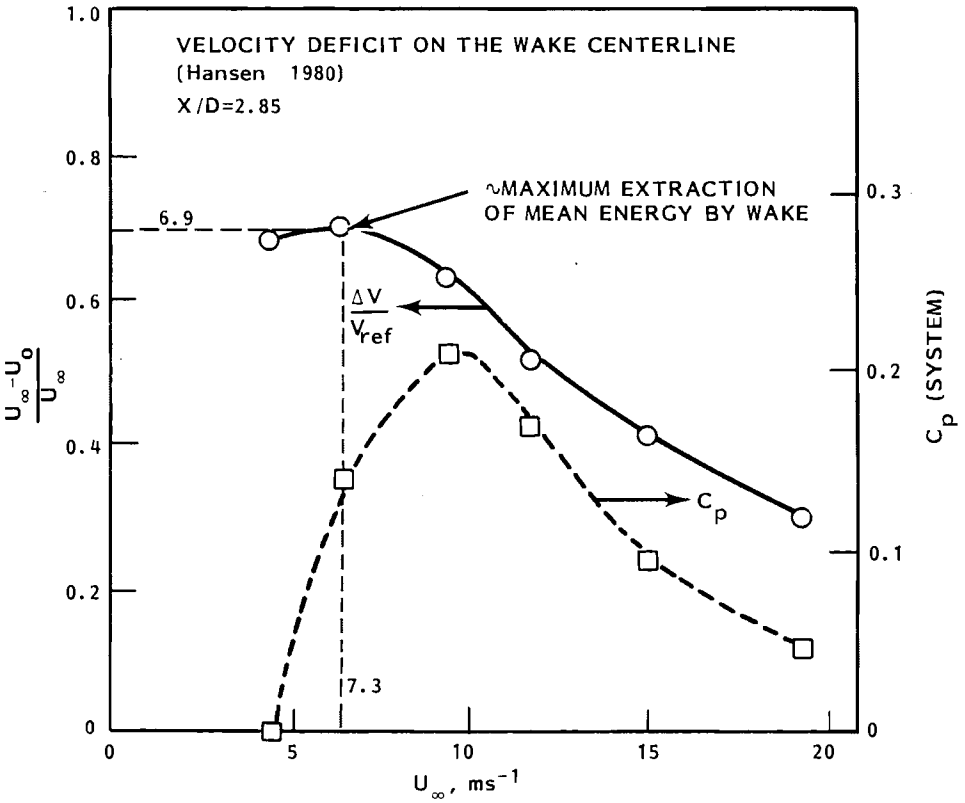

FIGURE 3. Nondimensional wind speed deficit at x/D = 2.85, in the wake described in Figure 2, as a function of free-stream wind speed, U_∞. (Adapted from Hansen 1980, Figure 10).

energy as it applies to arrays of wind turbines. One needs to know whether the profile of wake wind speed can be known accurately enough to permit an optimization of these two factors. Wake studies are required for this purpose.

The present report describes the measured characteristics of a wake from the MOD-0A1 at Clayton, New Mexico, using 18 anemometers on the seven-tower VPA. A single case study of a wake is presented to provide an example of the nature of the wake of a 38-m diameter wind turbine, to show the kinds of analysis that are possible, and to indicate the possibilities and limitations for field study of wakes of real large wind turbines. The limitations and capabilities of some simple models of wakes are also shown.

2. THE FIELD STUDY CONDITIONS

The location of the anemometers relative to the MOD-0A1 wind turbine when the turbine nacelle axis passes through the center of the seven-tower VPA 2 diameters downwind of the rotor is shown in Figure 4. The wake is analyzed primarily using anemometers 8, 1, 2, 14 on tower D for vertical profiles and anemometers 11, 15, 16, 1, 17, 18, and 5 at hub height for the horizontal profiles. Each anemometer measures the axial wind velocity component and the horizontal and vertical cross-axis components. The length constant, representing anemometer response to fluctuations in wind speed, is 3 m. Smaller spatial variations of wind velocity are not measured accurately, although, if intense enough, they may be sensed by the anemometers.

A 17-minute segment of a longer record of wind velocity and turbine parameter measurements starting at 1005 MST on December 3, 1981, was selected for finding a suitably steady wake condition. The temperature layering was (buoyantly) neutral. Graphs of wind speed and turbine parameter values as a function of time throughout the 17-minute period are shown in Figure 5. In order to reduce the number of unwanted varying wind parameters, two subsegments of the total time period with particularly steady turbulence were selected at 0 to 4.27 minutes and 7.5 to 12 minutes. Of these two periods, the first one (period Ia) was selected for the present analysis as being the most steady. During this period, the wake was most symmetrically impinging upon the vertical plane array of anemometers. The turbine was very close to rated power (200 kW) during most of period Ia. Figure 6 contains plots of axial wind speeds at the array and turbine parameters versus time for period Ia.

The average values of the components of wind velocity at all points on the VPA for period Ia are shown in Figure 7. Estimates of average values of selected MOD-0A1 parameters are shown at the bottom of Figure 7. The U-direction wind speeds in the array-like plot indicate that the wake impinged nearly symmetrically upon the anemometer array. Typical hub-height axial wind speed spectra in the wake at the VPA are shown in Figure 8. These spectra do not

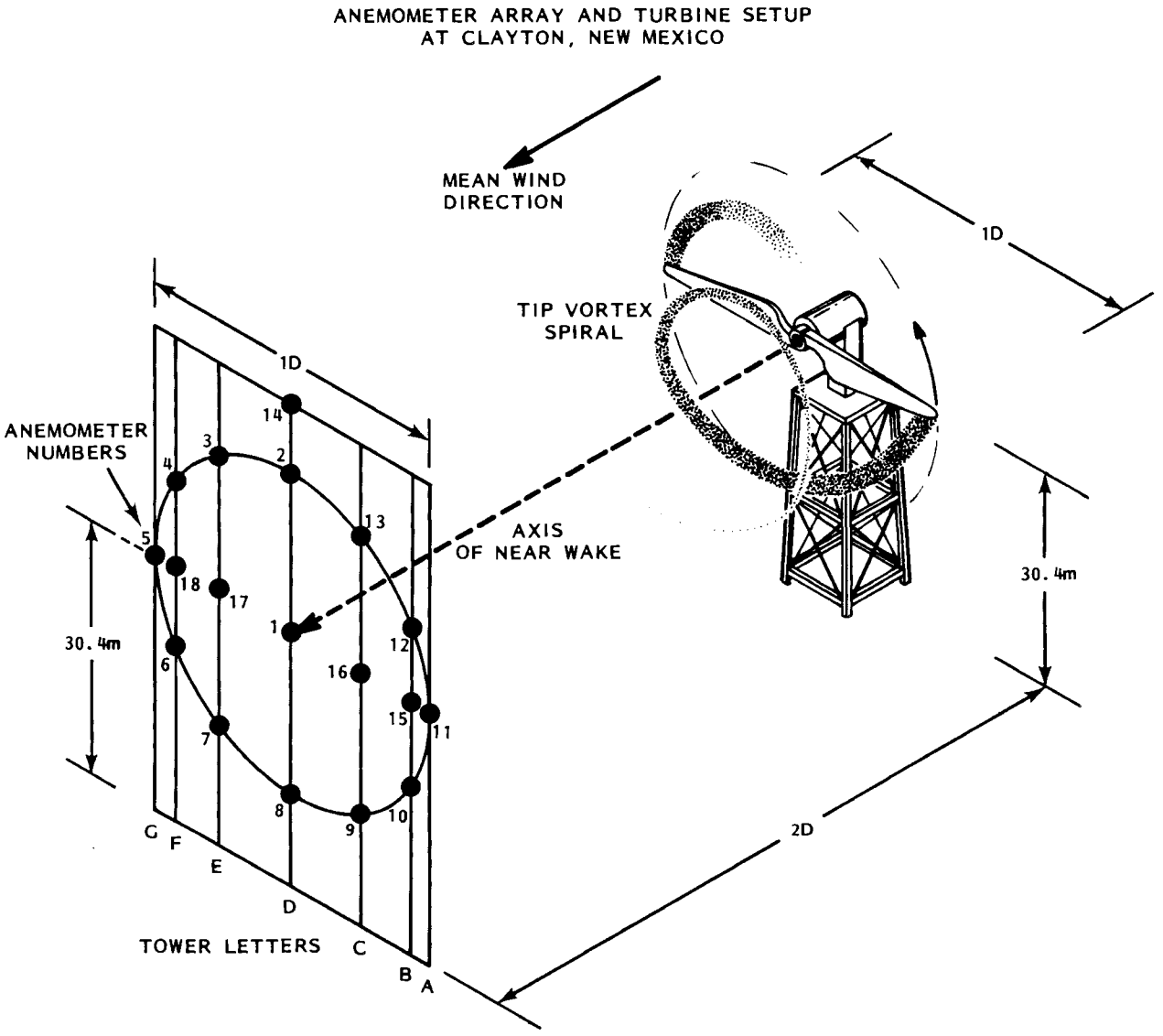

FIGURE 4. An oblique schematic view of the Clayton, New Mexico field study configuration of the VPA and the MOD-0A1 turbine for wake measurements on December 3, 1981.

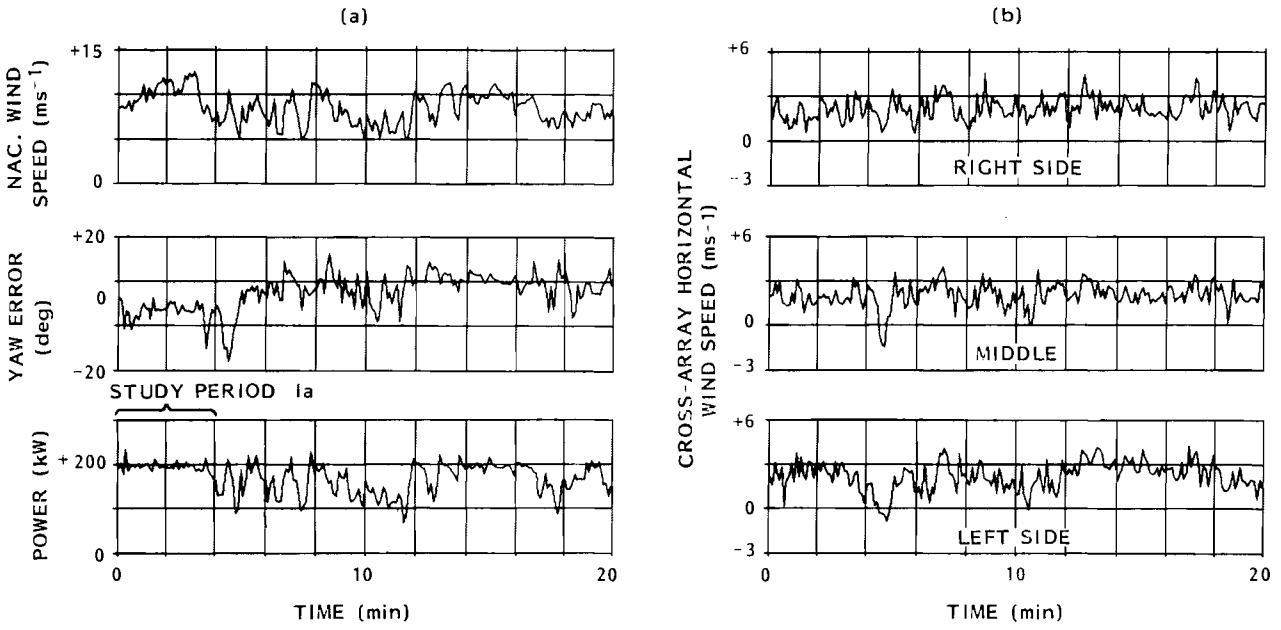

FIGURE 5. Graphs of measured wind turbine parameters and VPA-measured winds surrounding the time selected for study of the turbine wake on December 3, 1982: a) turbine parameters; b) horizontal cross-array wind velocity at hub height on the right, center and left locations of the array looking into the wind.

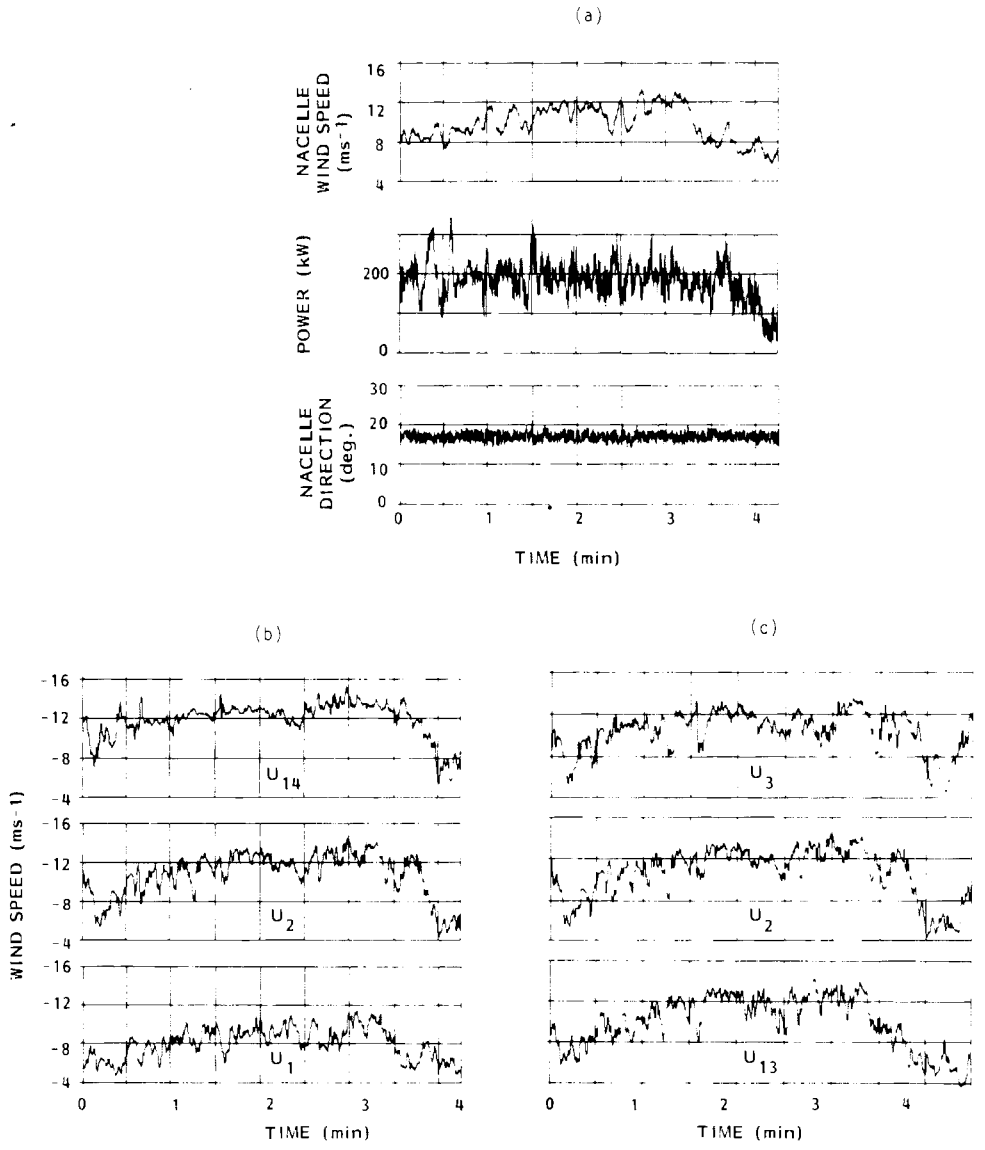

FIGURE 6. Expanded graphs of selected variables measured during the selected study period Ia: a) turbine parameters, b) and c) axial wind speeds at positions 1, 2, 3, 13 and 14 on the VPA; d), e) and f) axial wind speeds at positions 5, 6, 7, 8, 9, 10, 11, 12 on the VPA.

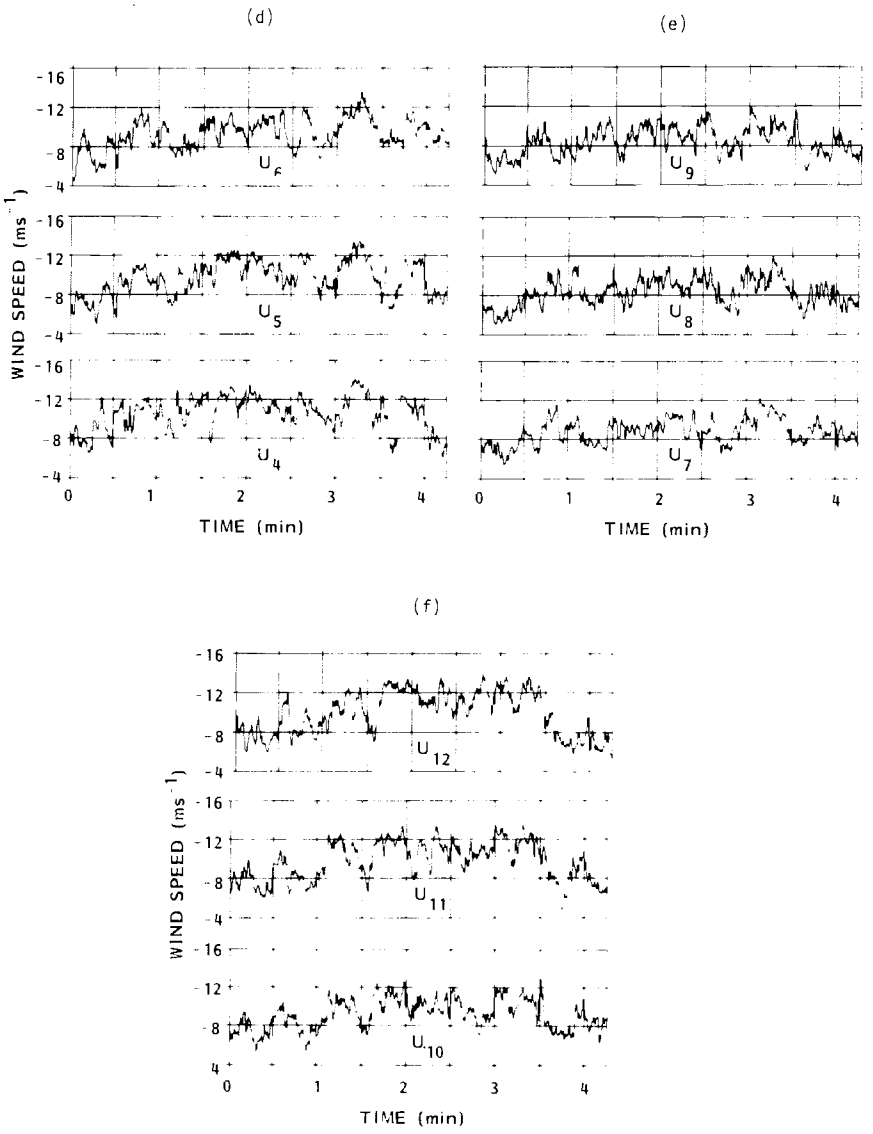

FIGURE 6. Continued

VERTICAL PLANE ARRAY VELOCITY COMPONENTS FOR 4.27 MINUTES
OR 1024 DATA POINTS ENDING AT 4.26 MINUTES

U-DIRECTION, m/s

			-11.85						
			-10.76						
		-10.44		-10.17					
	-10.54				-9.84				
-9.72	-10.06	- 8.89	- 8.05	- 9.00	-9.46	-9.71	9.75		
	- 9.25				-9.20				
		- 8.79		- 8.38					
			- 8.33						

WIND SPEED, m/s

			12.14						
			10.82						
		10.55		10.21					
	10.67				9.90				
			8.11						9.77
	9.30				9.20				
		8.86		8.38					
			8.35						

V-DIRECTION, m/s

			- 2.63						
			- 1.16						
		- 1.55		- 0.90					
	- 1.70				-1.06				
-0.70	- 1.22	- 0.92	- 1.04	- 1.10	-0.18	-1.10	20.86		
	- 0.90				-0.23				
		- 1.11		- 0.17					
			- 0.61						

RESULTANT WINDS
DEGREE FROM NORTH

			12.47						
			18.85						
		16.58		19.93					
	15.83				18.88				
			17.62						18.56
	19.44				23.59				
		17.81		23.86					
			20.79						

VERTICAL, m/s

			0.94						
			0.16						
		0.27		- 0.08					
	0.43				-0.17				
-0.01			0.34			-0.01	1.75		
	0.36				-0.01				
		0.00		- 0.16					
			0.64						

TURBULENCE
σ_u, SIGMA OF U COMP., m/s

			1.83						
			2.31						
		1.89		2.35					
	1.74				2.21				
			1.62						1.97
	1.58				1.59				
		1.30		1.45					
			1.41						

AVERAGE VALUES OF MOD-OA PARAMETERS
(NO ACCURATE CALIBRATION)

CHORDWISE BENDING MOMENT AT STATION 40 = 0.881×10^5 ft lb	POWER = 192.34 kW
FLATWISE BENDING MOMENT AT STATION 40 = 1.52×10^5 ft lb	NACELLE DIRECTION = 17.11 deg
BLADE PITCH = -4.87 deg	NACELLE YAW ERROR = -3.41 deg
ROTOR RPM = 41.32	NACELLE WIND SPEED = 9.81 m/s

FIGURE 7. Average wind velocity components, the rms of axial turbulence and turbine parameters over period Ia. The wind values measured from the array are plotted in a slightly distorted (diamond) representation of the VPA ring geometry.

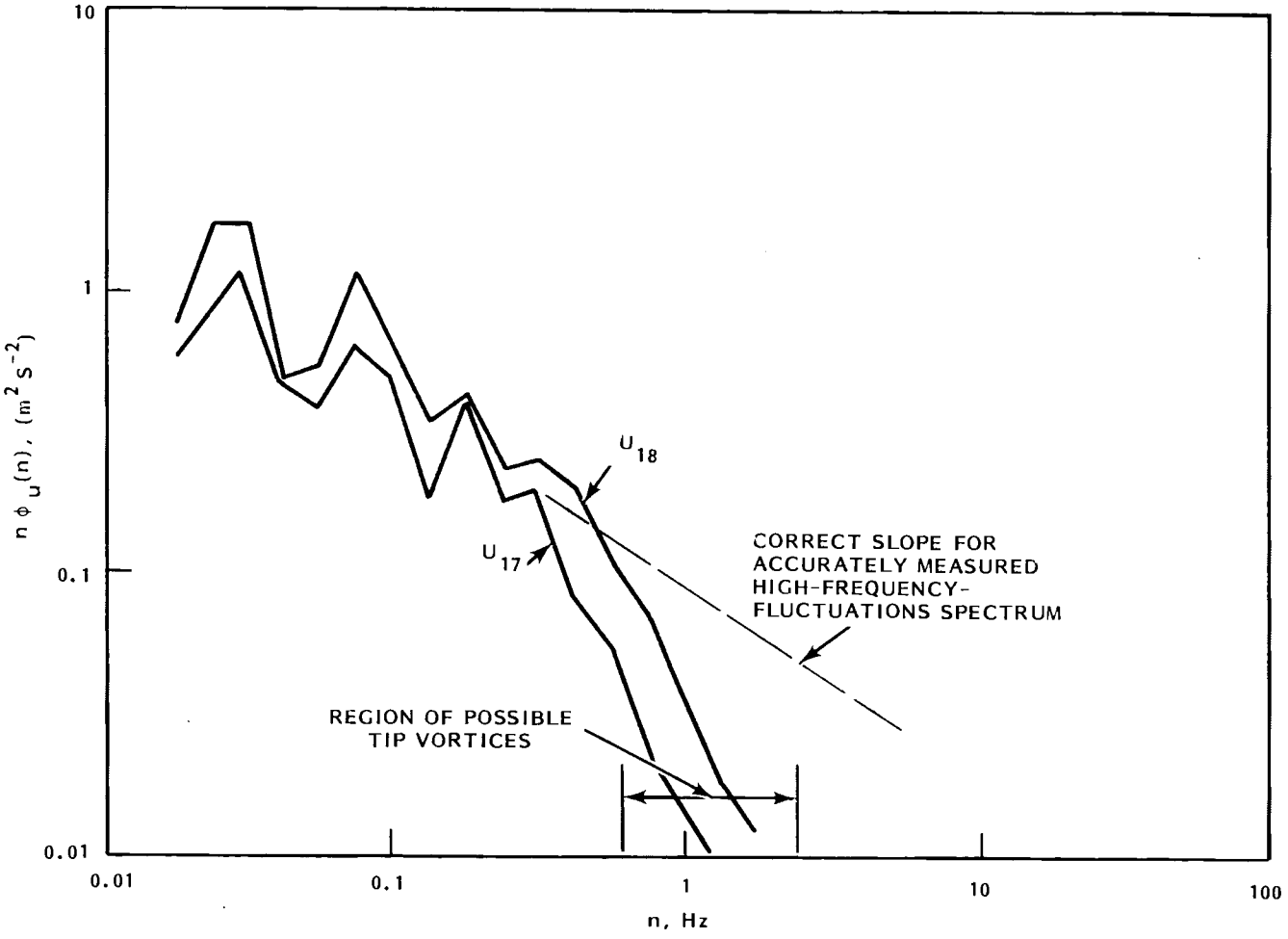

FIGURE 8. Power spectral density curves of axial wind speed at two hub-height locations on the VPA during the study period Ia.

show the full magnitude of the existing small-scale turbulence but should indicate the existence of a significant energy peak if the tip vortex impinged upon the anemometer during the whole period. No such peaks are indicated in the figure.

The VPA was designed primarily to measure wind throughout the plane when the wind was blowing from the array to the turbine. Thus the anemometers were placed on booms which extend from the seven towers in a direction away from the turbine. When a turbine wake exists at the VPA then it might be assumed that the array anemometers also are affected by the wakes of the towers which support them. It can be shown that, in the present study, there is not a significant error in the measurements. Figure 9 shows that the anemometer booms were oriented 40° to the west of the direction of the normal to the VPA. Further, the boom tips and anemometers are 4.5 tower widths (W) from the tower. That these conditions lead to a minimal error in measurements of turbine wakes whose axes are through or to the east of the center of the VPA is evident from the plots of tower effects on wind measurement shown in Figure 10, which is adapted from Gill et al. (1967). The lower polar diagram has a tower of the shape that corresponds to the anemometer and tower configuration used in the VPA. The upper polar diagram gives the magnitudes of the observed-speed factor for boom lengths 2 and 4 W. It should be noted that these curves are said to be characteristic and to permit reasonably accurate interpolations between them. Since it has not yet been possible to calibrate the VPA towers for their influence by making the needed measurements, previously published data must be used to estimate the errors introduced. Considering the diagrams in Figure 10 and the fluctuating nature of the turbine wake wind, it appears that the required correction will be sometimes negative and sometimes positive and probably never more than 5% for the direction of the wake encountered in the present study and the length of boom used.

We therefore assume that the errors in 4.27-minute average wind speeds are negligible. At any rate they are likely to be of similar sign and magnitude at all anemometers so that errors in the shape of the measured wake profiles

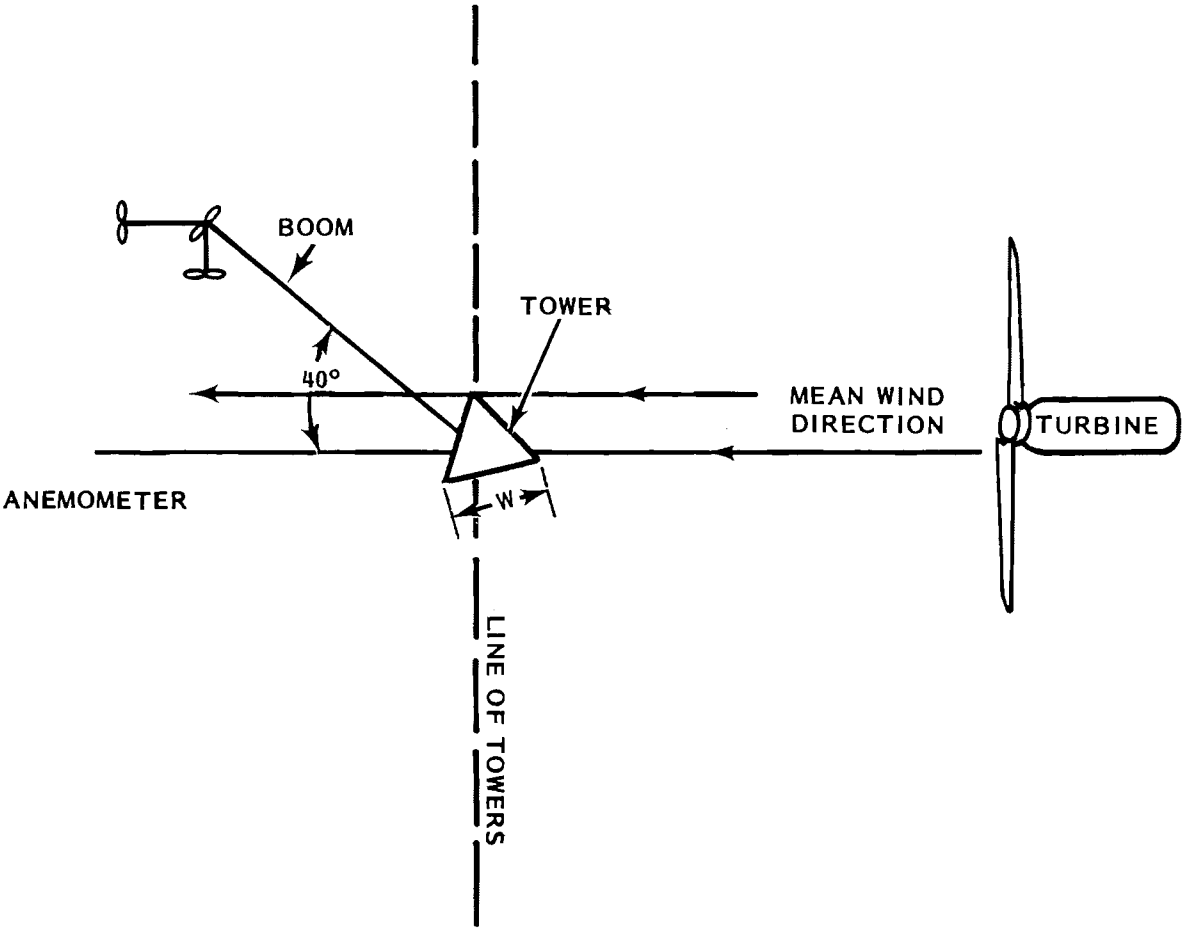

FIGURE 9. Map view of the location of each individual anemometer propeller relative to its support tower and to the wind turbine and wind direction for a turbine wake case.

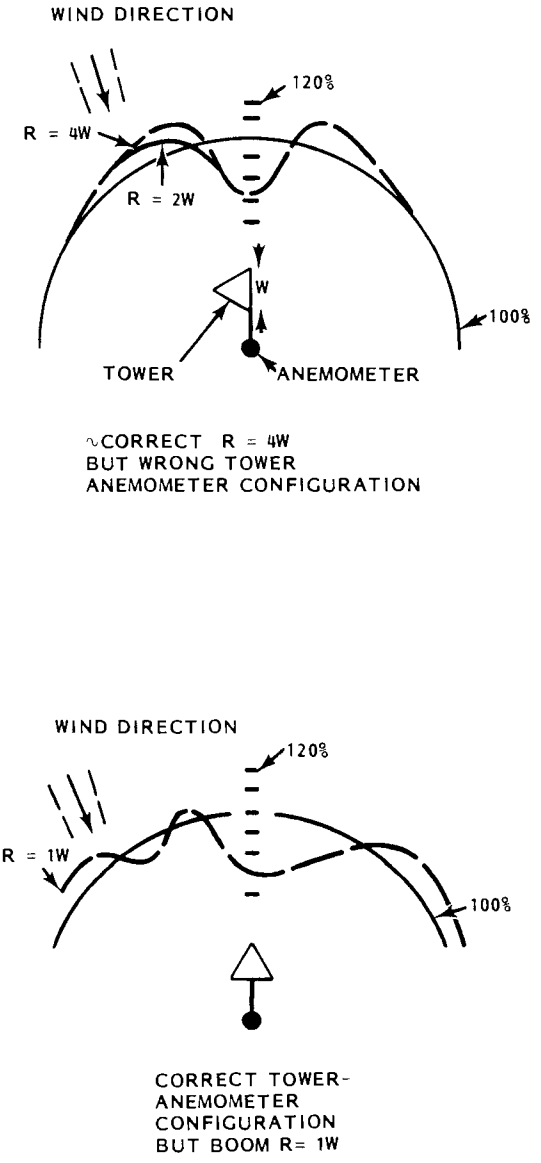

FIGURE 10. Polar diagram of the percent of correct wind speed that will be measured by an anemometer located near its boom support tower as a function of wind direction. The wind direction for the study period Ia is indicated by an arrow and two dashed surrounding lines. (Adapted from Gill et al. 1967).

will be smaller. The effect of the 0.5 m diameter towers on the estimated spectra of turbulence will be minor since the propeller anemometers respond only weakly to turbulence lengths of 3 m and less. The characteristic length of turbulence generated by the anemometer tower is 0.5 m or less.

3. WAKE MEAN AXIAL WIND AT X/D = 2

At hub height, 30.4 m above the ground, there are seven anemometer locations across the wake. The map in Figure 11a shows that, on the average, the wind turbine axis points 7° to the tower A side of the center of the tower array. The wind at the center (labeled D) tower also has a 7° cross-axis direction on the average. This is approximately true at tower A, but at tower G the wind direction is 4.1°. This suggests a half-angle spread rate for wind in the wake of from about 1° to 3°. Similar computations at the top and bottom anemometers of the center tower suggest an upward movement of air at an angle of 4.4°. The average half angle of horizontal lateral spread of the wake from the turbine to the VPA may be estimated by considering the wind profile in Figure 11b. The 95% recovery of wind speed in the tail of the profile occurs at a radius of 32 m. The angle of spread from the rotor disc edge to this radius in the wake at x/D = 2 (the half angle for a symmetric wake) is 9.6°. A 4° half angle of spread is calculated using the radius to the 75% recovery wind speed in the tail of the profile to define the edge of the wake.

Figure 12 contains the vertical profile of wake wind at the center tower. The 95% recovery in the vertical profile is at an average radius of 24 m, resulting in a half angle of spread of 3.7°. There is much less angular difference between the 95% and 75% edges in the vertical profile than in the horizontal profile.

The mean values of cross-axis components of the wind, V and W, are distributed across the array in a pattern of values that is consistent with the existence of rotor-induced swirl in the wake. The plots in Figure 7 are such that the viewer is looking into the direction from which the wind blows (i.e., the viewer is standing in the wake looking at the turbine and VPA). The turbine rotor would appear to be turning counter-clockwise. An examination of the array of vertical velocity values reveals that the wind in the wake moves upward on the left side and downward on the right side. This is equivalent to a clockwise swirl. In the vertical direction the variation of V is

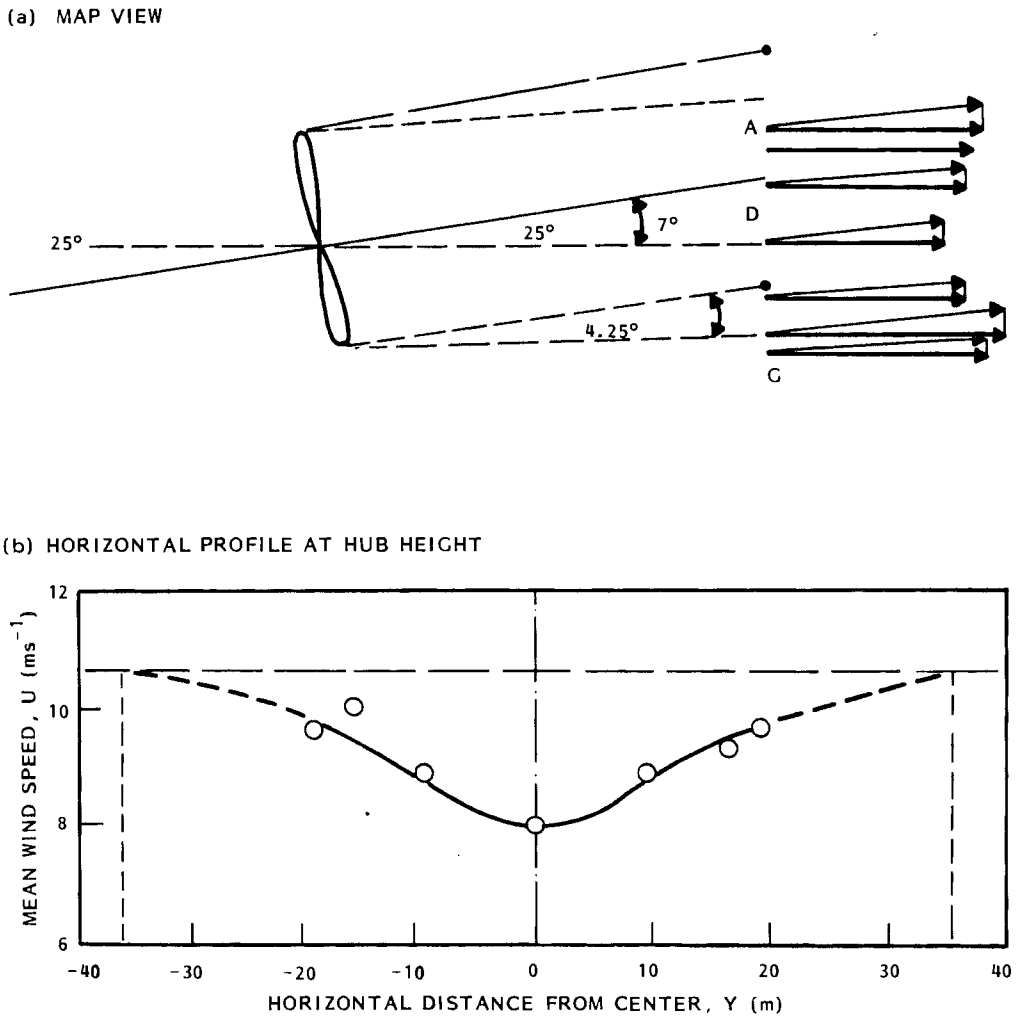

FIGURE 11. a) Horizontal geometry and mean wind speeds for the turbine and wake measurements at the VPA. Note the 7° displacement of the turbine from the array axis. b) Cross-wake horizontal profile of mean wind speed of the wake of the MOD-0A1 at x/D = 2.

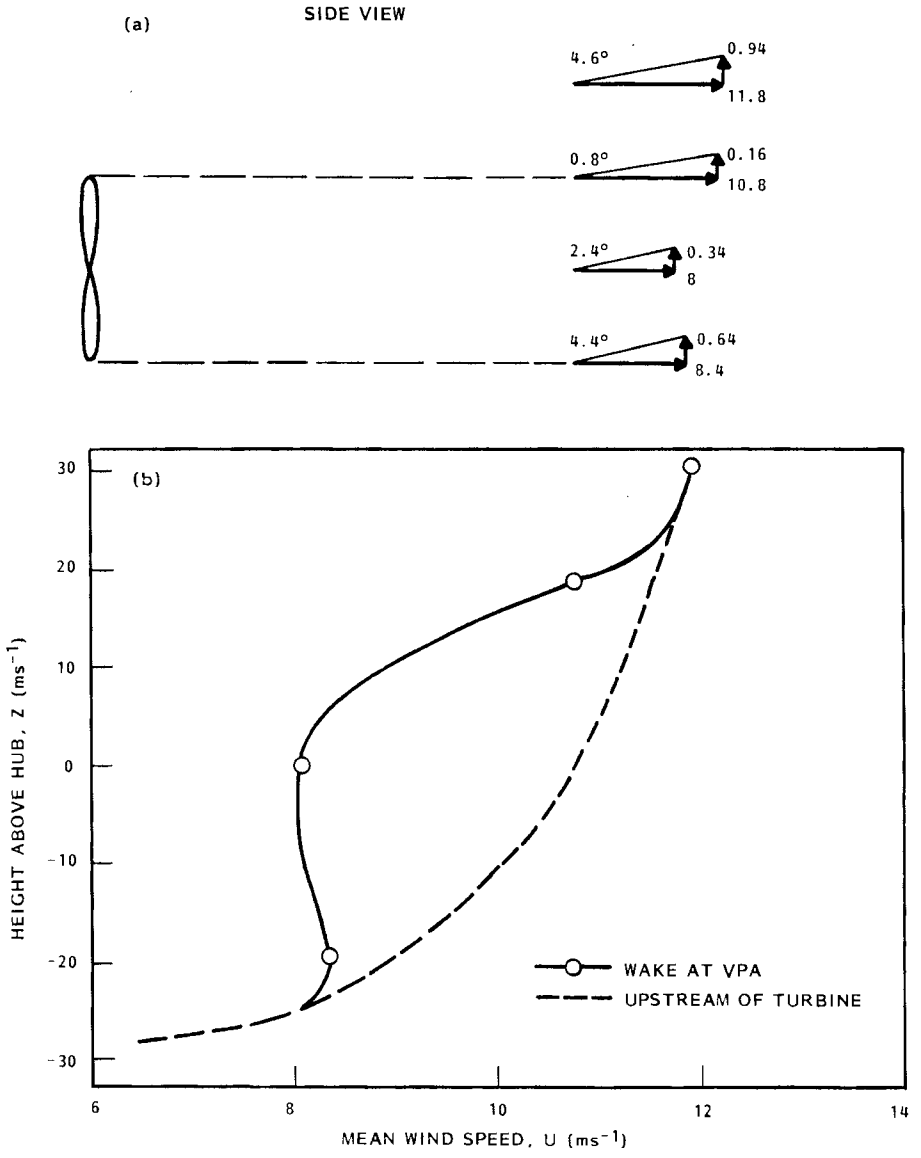

FIGURE 12. Vertical geometry and center-tower profile of the mean wind speed of the wake at x/D = 2: a) orientation of the mean wind components in the vertical plane through the array axis; b) wake profile (upwind profile is indicated by the dashed line).

also consistent with clockwise swirl of about the same magnitude. The maximum swirl rotation rate at a radius of 19 m was measured to be about 0.025 rad s^{-1}.

The maximum wake deficit at x/D = 2 was 2.7 ms^{-1}. The resulting nondimensional deficit is

$$\frac{(U_\infty - U_0)}{U_\infty} = 0.25 \ .$$

The turbulence characteristics of the wake are described in the next section.

4. TURBULENCE IN THE WAKE AT X/D = 2

An examination of spectra of turbulence measured at each point of the vertical plane array is instructive about the character of the wake. Figure 13 contains spectra measured for the seven locations at hub height and three additional locations on the center tower (D) of the array. The spectral plots are placed approximately at the positions of the corresponding anemometers on a drawing of the array. However, the spectrum from the 61 m location on tower D above the disk of rotation is placed unsymmetrically in the figure. The spectrum for the U component of wind is plotted as a solid line at each location. At the outer ring, which represents the path of the rotor tips, the vertical velocity spectra are included as dashed lines. All three wind-component spectra are shown at the central location and the 61 m, tower D (anemometer 14) location. Refer back to Figure 8 and recall that the spectral slope at frequencies greater than n = 0.7 Hz is not accurate due to the large anemometer length (or time) constant. Inspection of the axial wind speed spectra (solid lines) in Figure 13 reveals that the spectral maxima are greatest at the edge of the wake (U_2, U_5, U_8 and U_{11}). These peaks diminish in magnitude in a regular way toward the center of the array (U_1). The anemometer at position 14 on the top of the center tower is apparently outside the edge of the wake since its U spectrum peak, shown in the upper right hand graph in Figure 13, is also low. Also U_8 appears to be only slightly within the bottom of the wake.

Two other spectral features appear to be related to the wake. One is the appearance, in the left wake edge particularly, of peaks at about n = 0.25 Hz and 0.5 Hz (see arrows for U_{17}). At a wind speed of 10 ms^{-1} this implies a length scale of 40 and 20 m, or about 1 D and 0.5 D. A second feature is the u-spectral spike at about n = 0.025 Hz. This appears at all locations in the disk of the VPA but not at the 61 m location above the circle (anemometer 14). This peak is consistently higher at the four ring locations (closest to the edge of the wake) and diminishes toward the middle of the wake. Using the

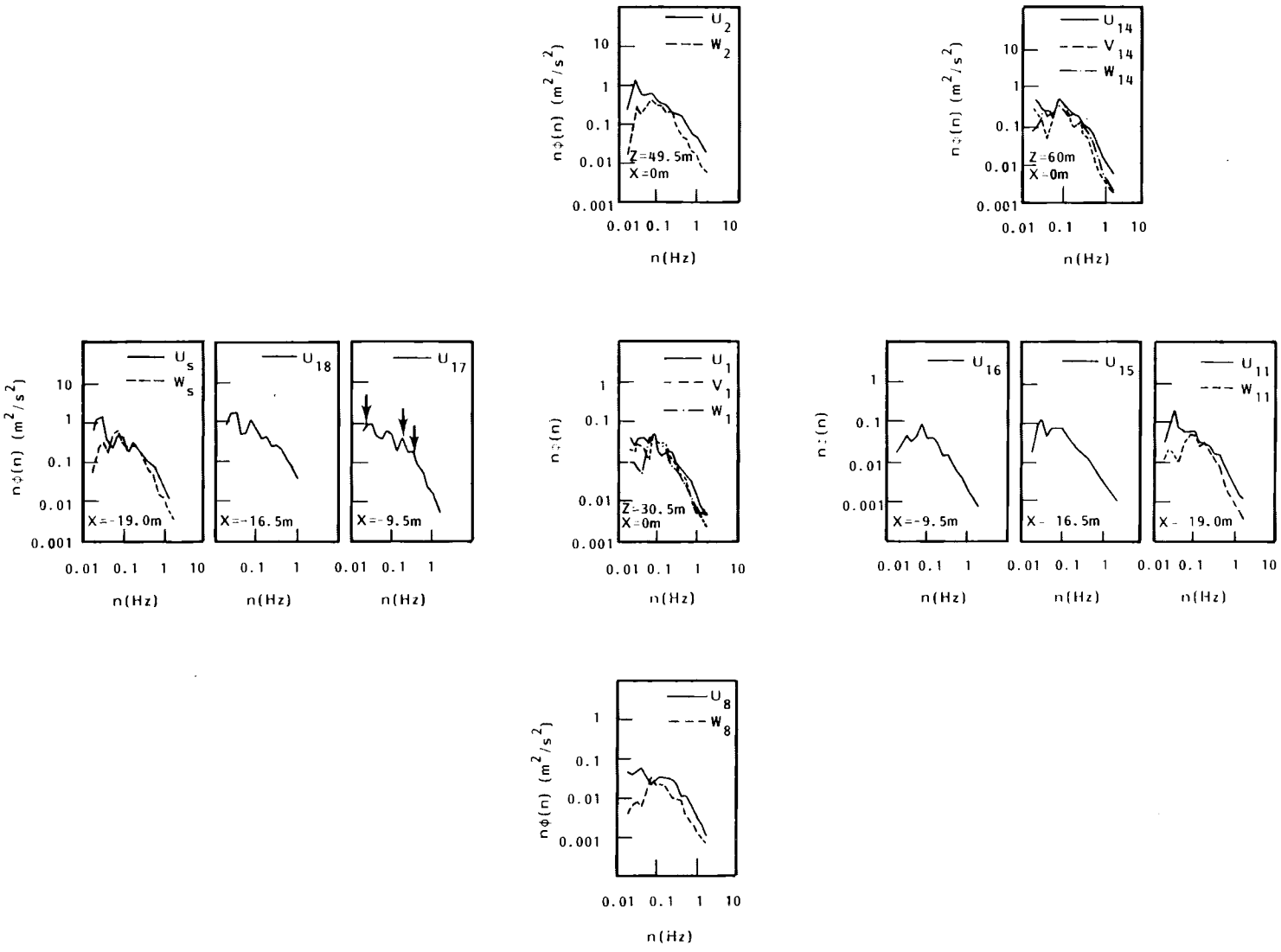

FIGURE 13. Spectra of wind speed at fixed positions on the VPA for study period Ia. Each spectrum graph is labeled by a letter representing the wind component and a subscript representing the anemometer location. (See Figure 4 for locations.) The horizontal set of graphs are at the hub height for all array towers level. The extra three graphs complete the set for all heights on the center tower.

advection calculation, as done for the higher frequency peaks, a length scale of 400 m is indicated. This probably represents a meandering of wake direction with a period of about 40 seconds or some oscillation of the wake, either axially or laterally (which may not have the length scale indicated, but only the time scale).

It appears that the spectral analyses of wake winds detect several rotor-scale eddies at about 0.25 and 0.5 Hz or length scales of 1.0 and 0.5 D. Further, a possible oscillation in the wake on a larger scale is indicated. The principal author has observed building wake bubbles to extend and contract with similar time scales.

One might expect to find some indication of tip vortices at the edge of the wake by peaks in the spectra at n = 0.67 Hz (1 P) and at n = 1.33 Hz (2 P). There are only hints of such peaks at the edges of the wake at anemometers 2, 5 and 8 and possibly at 1, 16, 15 and 11. These data have been averaged to give eight spectral points per decade of frequency, which will smooth out narrow spikes. To assure that we do not overinterpret the data consider the spectrum in Figure 14a. This is for U at position 1 in a nonwake case. No hints of spikes are in evidence in the 1 P or 2 P frequency locations. The spectrum was recalculated in two high frequency regions without the spectral smoother applied and plotted on linear scales. This fine-resolution spectral plot in Figure 14b shows no strong single spectral peaks at frequencies corresponding to 1 P and 2 P revolutions. The conclusion drawn is that no tip vortex is detectable spectrally at a distance x/D = 2 downwind from the turbine. The reason may be better understood by examination of a photograph of smoke tracing the tip vortex motion in the near wake of the MOD-0 turbine (Figure 15). The essential point here is that the tip vortex breaks down into broader band turbulence within one to two rotor radii downwind of the rotor in the turbulent boundary layer.

One aspect of the problem of turbine-turbine interaction is the turbulence experienced by a second turbine in the wake of the first one. It has been shown by the principal author that the spectrum of turbulence seen by a rotating

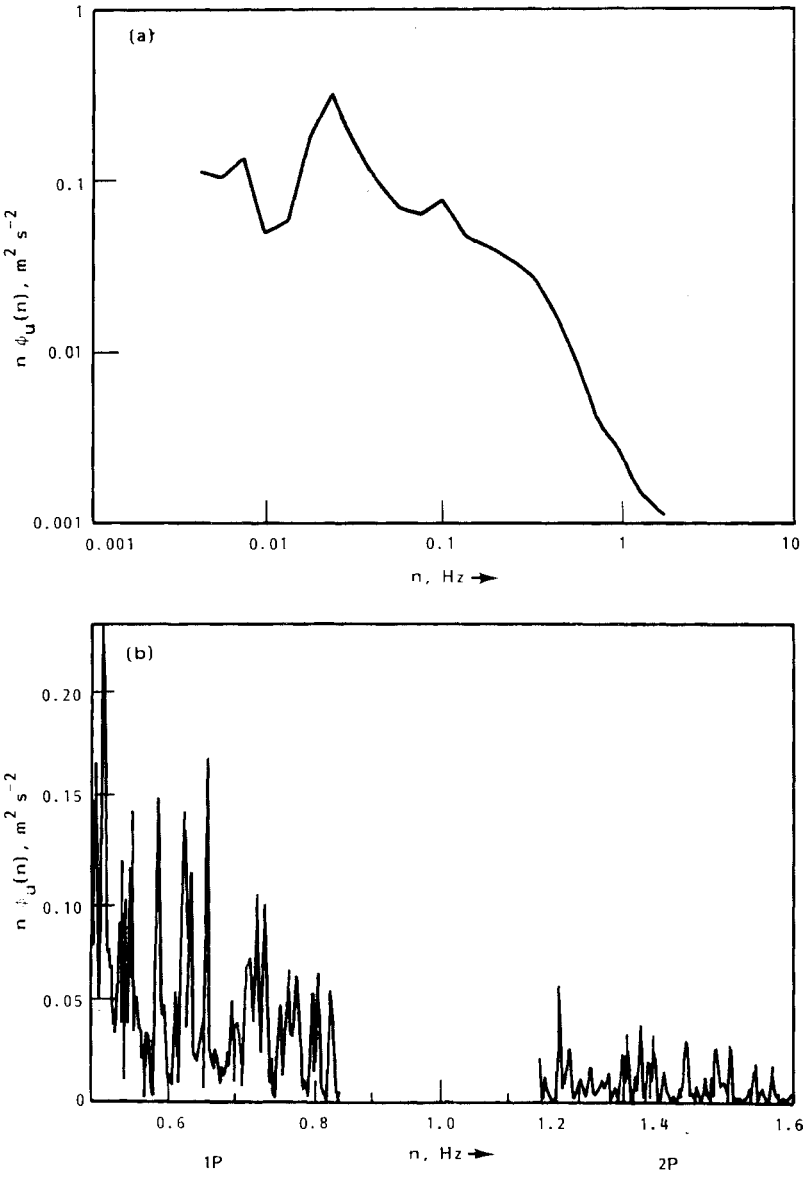

FIGURE 14. Spectral assessment of the existence of a tip vortex at x/D = 2: a) spectrum of axial wind speed at hub height for a nonwake case; b) spectrum of the same component of wind on the left edge of the wake at hub height. (The data in the gap of spectrum (b) is not plotted since it is far from the 1P and 2P regions. No vortex peaks appear in spectrum (b).)

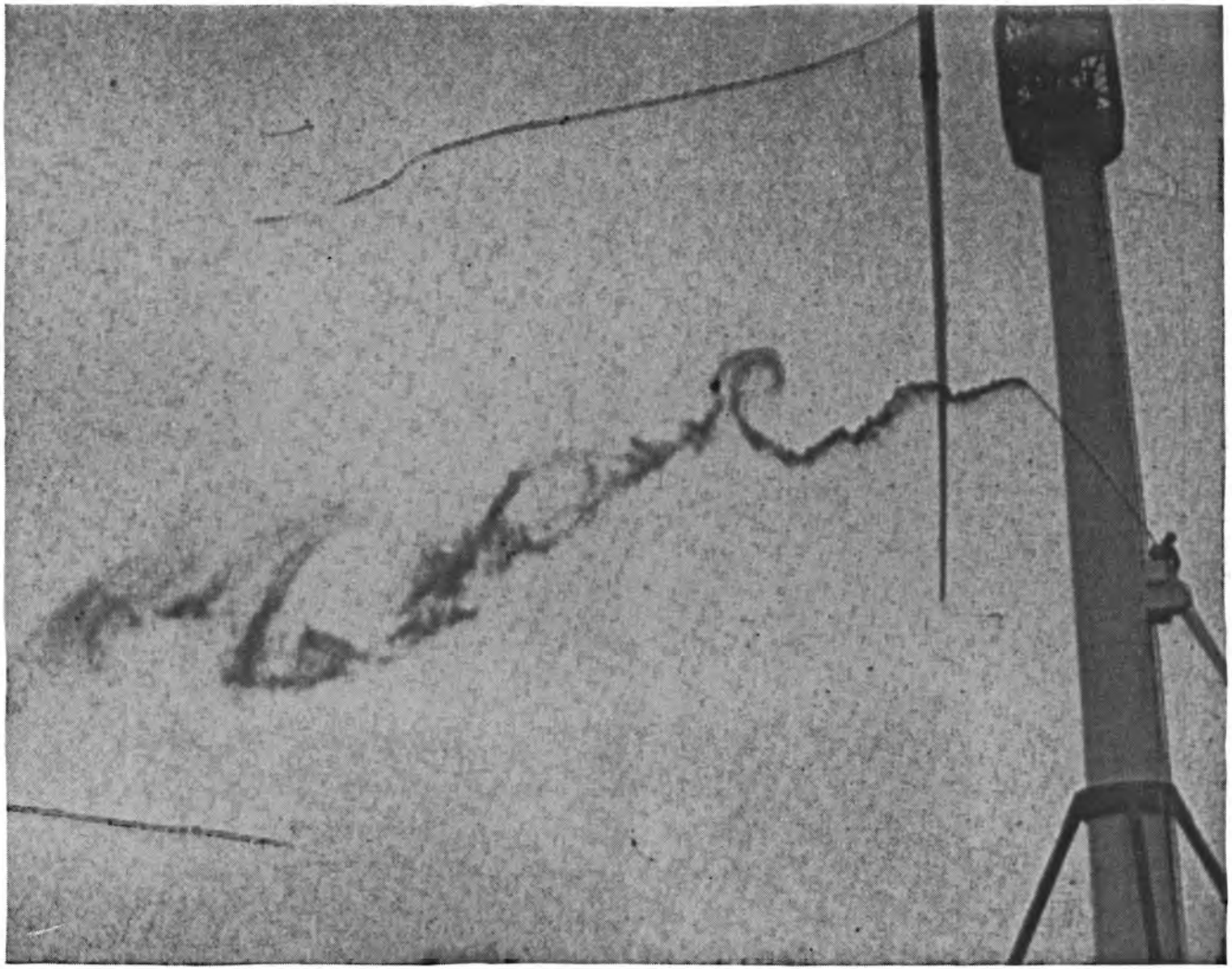

FIGURE 15. Photograph looking up from the side into the MOD-0A1 turbine wake, showing the tip vortex trace by smoke. Four members of the vortex sequence are shown. The structure of the vortex has broken and mixed into turbulence within the 1D distance shown.

blade is properly estimated from a rotationally sampled time series of wind speed (Connell 1981). The rotationally sampled wind has been derived from VPA data for the present wake case and the resulting spectrum is shown in Figure 16a on a logarithmic graph. Although no corresponding rotational spectrum from the upwind free stream was measured, it appears that the spectrum is not radically different in the wake than might be expected away from the wake. Any differences are most likely to be found in the details of the spectral spikes at frequencies near or above n_o = 0.67 Hz (1 P). Figure 16b shows the fine resolution form of the spectrum for this high frequency region on a linear plot. The spikes corresponding to 1 P, 2 P and 3 P rotation frequencies are seen to be about 0.2 Hz wide for the 4.27 minute period of measurement. The peak energy density is quite large. A nonrotational spectrum plotted on the same linear graph would appear as a spike near the zero value on this graph.

Crosswind horizontal and vertical profiles of turbulence energy and integral time scales in vertical and horizontal planes passing through the axis from the turbine hub to the VPA center anemometer are plotted in Figure 17. The integral time scale is a measure of the periodicity of the largest turbulent eddies passing a fixed point. The standard deviation of the axial wind speed fluctuations measured at fixed points is plotted as the measure of turbulence energy.

The horizontal profile of the root-mean-square (rms) value of axial wind speed fluctuations, σ_u, shows a maximum at the wake edge and a deficit relative to the wake edge, $\Delta\sigma_u$, of 0.5 ms^{-1}. The profile shape suggests an asymmetry in turbulence mixing and generation in the wake. The intensity of turbulence, σ/U, is in the range 0.2 to 0.15. Integral time scales of the axial turbulence were computed from autocorrelations. The time scales are a bit large to be for the ambient atmospheric boundary layer at 30.4 m above the ground. The largest scales are observed in the central region of the wake; the smaller scales are observed in the edges of the wake. The integral scale profile appears to be more symmetric about the nacelle center line than do the V, W and σ_u profiles.

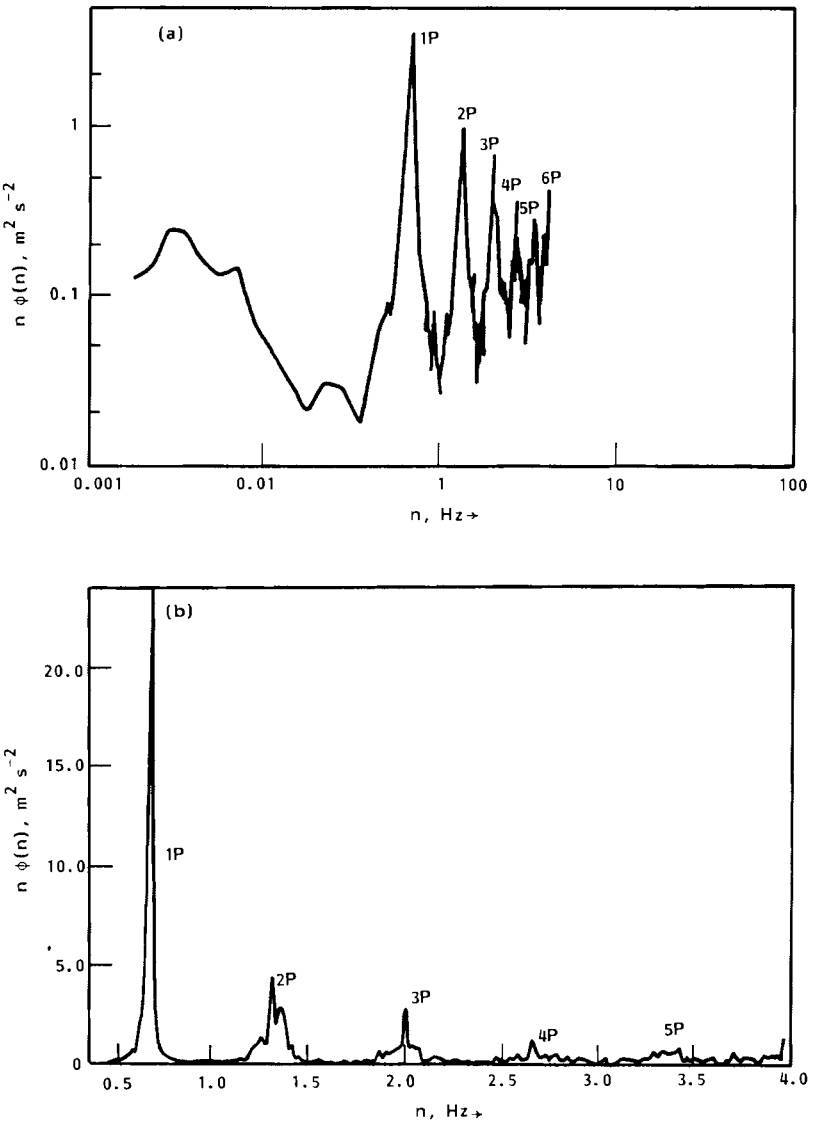

FIGURE 16. Spectra of axial turbulence that would be experienced by a MOD-0A operating 2 diameters directly downwind of the MOD-0A1 at a hub height mean wind speed of U_H = 10 ms^{-1}: a) logarithmic-scale plot; b) linear-scale plot expanded to resolve the high frequency portion of the spectrum. Spectra computed from measurements in the wake on December 3, 1981.

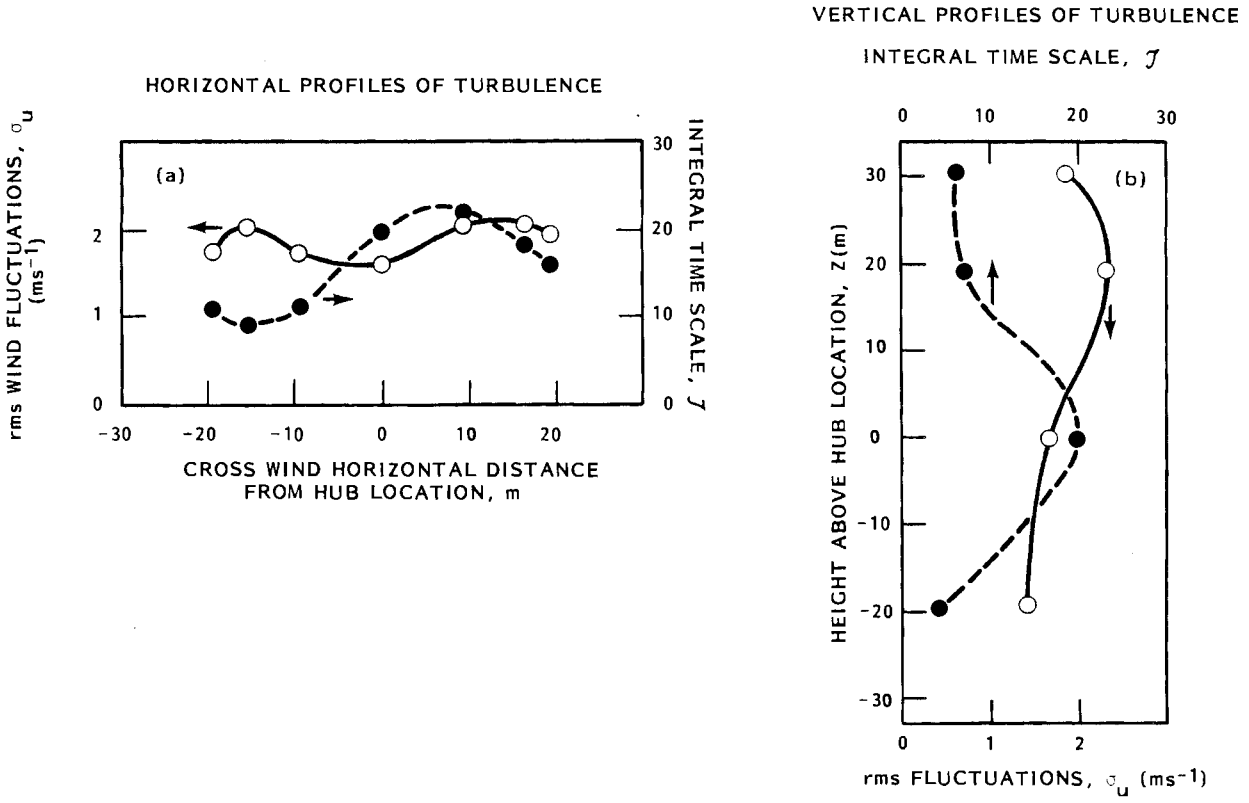

FIGURE 17. Profiles of turbulence properties in the wake of the MOD-0A1 at x/D = 2. Symbols: O root mean square axial wind speed fluctuations; ● integral time scale of the axial wind. Figure 17a contains the crosswind horizontal profiles through the center of the VPA. Figure 17b contains the vertical profiles through the center of the VPA.

The vertical profile of σ_u suggests rather uniform turbulence energy except for an increase near the top edge of the wake. As in the horizontal profile, the integral time scale is distributed more symmetrically about the nominal wake axis than are the other variables. The maximum time scale is at the center of the profile and the minima are at the wake edges. The values of the integral time scale at the top of the vertical profile appear to be more in line with those expected at that height in a natural boundary layer. The other values are large. They may reflect the meandering of the wake axis or variation of the length of the wake "potential core". Both of these phenomena have been observed by the principal author in field studies of wakes of buildings.

Using the time average characteristics of the turbulence displayed in Figure 17 as indicators of the width of the wake, about a 3° average half angle of spread is indicated. Perhaps the most certain conclusion is that turbulence in the wake appears to have been slightly more energetic than in the nonwake boundary layer. The time scales and possibly the length scales of turbulence were increased. This may not have a great impact upon stress on a second wind turbine placed in the wake.

5. COMPUTATION OF INDUCTION FACTOR IN THE WIND SPEED, ROTOR EFFICIENCY AND POWER COEFFICIENT USING WAKE DATA

The axial induction, or better, reduction, factor, a, in the wind speed for the average wake over the 4.27-minute period is estimated as follows (Wilson et al. 1976):

$$a = \frac{U_\infty - U_o \text{ (wake)}}{2\ U_\infty} = \frac{10.7-8.05}{2 \times 10.7} = 0.13 \ ,$$

where it is assumed that the maximum speed deficit of the wake at x/D = 2 is equal to the wake wind speed minimum at the point of pressure recovery. The efficiency, E, of the blades may be estimated as follows. Again, momentum theory assumptions are used.

$$E = \frac{P}{1/2\ \rho\ U_\infty^2\ AU_{rotor}} \ ,$$

where $U_{rotor} = U_\infty - aU_\infty$.

Then $$E \doteq 4a(1-a) = 0.46 \ .$$

$$C_p \doteq \frac{P}{1/2 A \rho U_\infty^3} = 4a(1-a)^2 = E(1-a) \ .$$

Then $$C_p = 0.40 \ .$$

The model MOD-0A reduction factor provided the author by T. Richards at NASA/LeRC has a value of a = 0.13 at U_∞ = 10 ms^{-1}. This compares with the present estimated value of a = 0.13 at U_∞ = 10.7 ms^{-1}.

6. A TWO-DIMENSIONAL DESCRIPTION OF THE WAKE

The VPA measurements make possible an estimate of the distribution of wind properties throughout the plane of the cross section at x/D = 2. A plot of values of wind deficit, $(U_\infty - U)$, using the complete set of anemometry locations on the VPA, is shown in Figure 18a. U_∞ is the upstream wind axial speed at the height of the wake wind speed value U. The solid lines represent estimated lines of constant deficit of different magnitudes. They delineate the cross-section shape of the wake. The deficits modified to include the extrapolated profile data, and nondimensionalized in the form $(U_\infty - U)/U_\infty$, are shown in Figure 18b. The wake is seen to spread more widely in the horizontal direction than in the vertical in the outer portions of the wake. The wake is about circularly symmetrical in the inner portions of the cross section at x/D = 2.

The flux of kinetic energy, E, orthogonal to the vertical plane at x/D = 2 in the wake is represented by the distribution of U^3 in the plane. The distribution of $2\ E/\rho = U^3$ is shown in Figure 19. The region of greatest deficiency of energy flux in the wake is seen to have been located in the inner half radius from the hub and near the ground for a second MOD-0A placed in the middle of this wake.

A subjective interpretation of these results suggests that the wake-reflecting effect of the ground was small at x/D = 2 and that horizontal spread was greater than vertical spread.

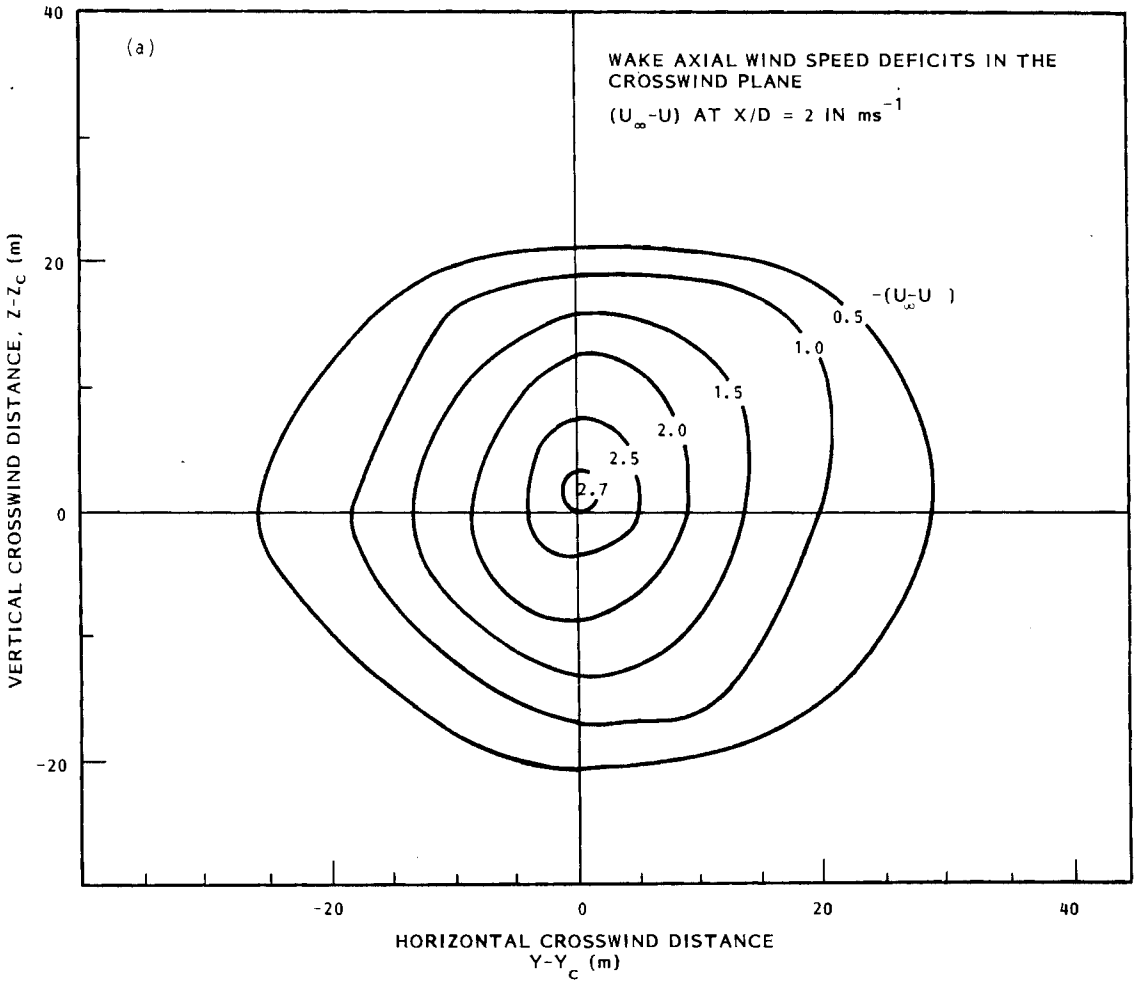

FIGURE 18. Two dimensional distribution of wake mean wind in the cross-axis plane at x/D = 2: a) wind speed deficit, $-(U-U_\infty)$; b) nondimensional deficit, $(-U-U_\infty)/U_\infty$ and the heavy solid lines represent lines of constant magnitude of the variable plotted.

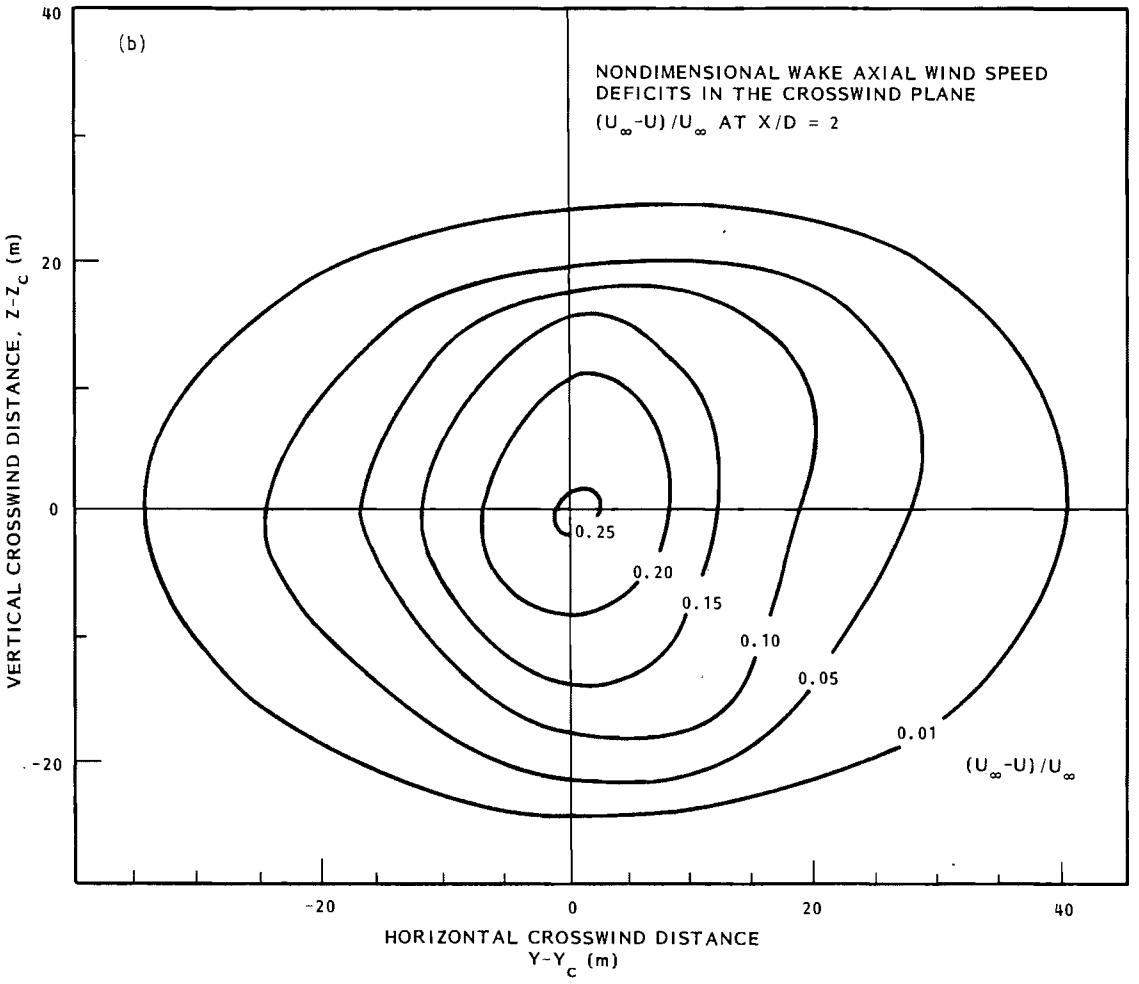

FIGURE 18. Continued

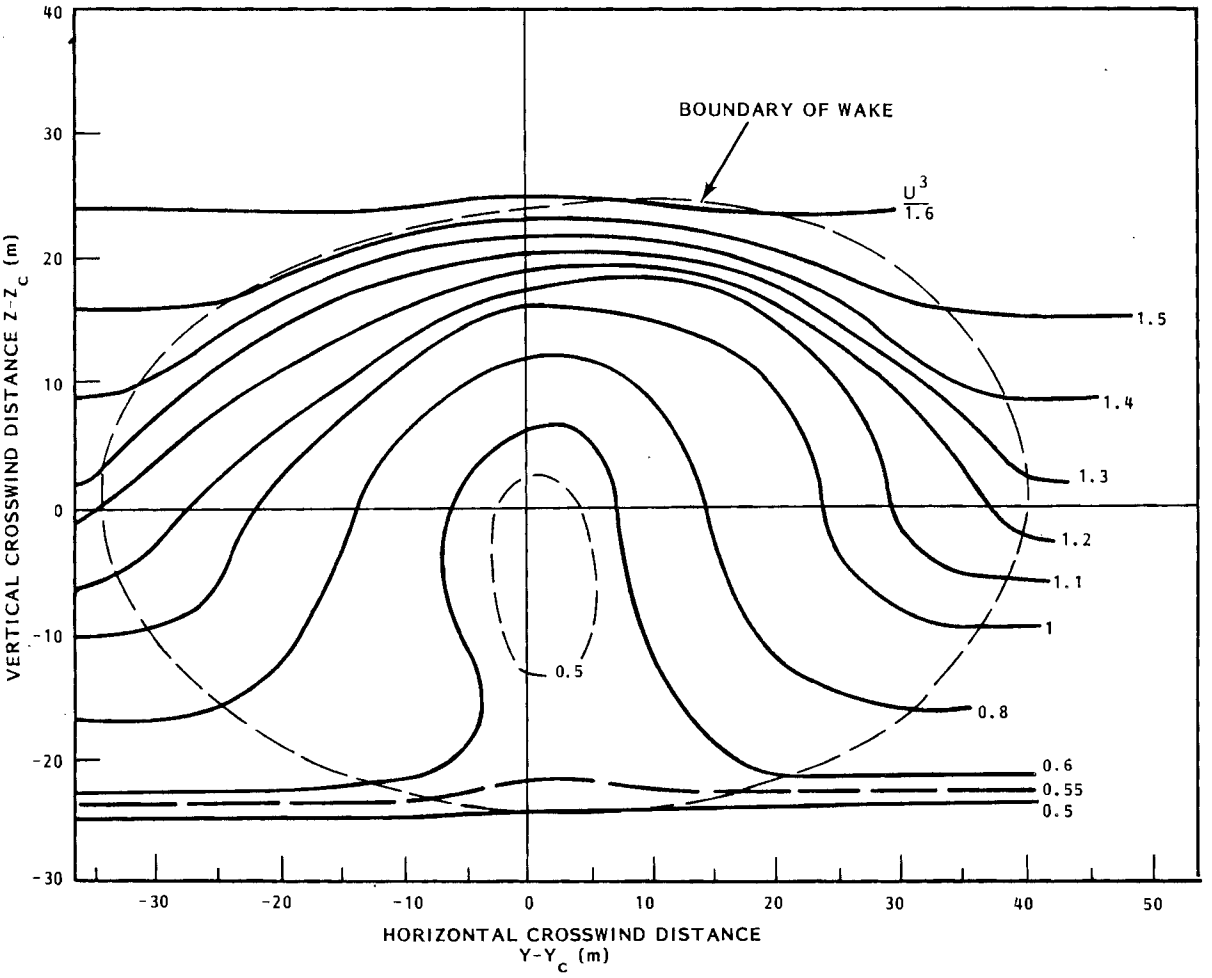

FIGURE 19. Kinetic energy flux per unit mass through the vertical crosswind plane of the wake, U^3. The heavy solid lines represent lines of constant magnitude of the variable plotted.

7. AN ESTIMATE OF AXIAL RATE OF REENERGIZING OF THE WAKE

The energy flux upwind of the turbine may be estimated using the vertical profile of U_∞. The energy flux through the wake cross section at x/D = 2 may be estimated using the data in Figure 19. The power out of the turbine generator was measured. The power train losses between the low-speed shaft and the generator are known rather accurately; we use a 91% efficiency of the power train. If reasonable estimates of loss of power in wake turbulence and swirl could be made, entrainment of ambient wind into the wake could be estimated. This would give us an average rate of recovery of the wake toward the nonwake condition for the interval x/D = 0 to x/D = 2. In practice this is difficult to do with the restricted amount of data available, but the exercise is instructive and is undertaken herein.

A schematic drawing of the airflow and the turbine processes involved in power extraction from the wind and in wake recovery is shown in Figure 20.

The wake mixes with the air just outside its boundary and effectively vanishes at some downwind distance. This reenergizing process of mixing is indicated by narrowing of the vertical separation between the dash-dot lines which enclose the region of significant wake defect. The dotted lines indicate the outer bound on the air flow that mixes into the wake in the region of x/D from the turbine to the point of contact of the dotted line with the wake boundary line. The inner wake region enclosed by the dashed line represents that portion that has not mixed at all with the environment. In a nonturbulent ambient wind case this would be called the potential core.

The following equation describes the balance between the power and energy flux contributions as air flows past an operating turbine.

$$A_1E_1 + A'E' = P_r + A_2E_2 \ , \qquad (1)$$

where

A_1 = crosswind area of upstream flow that passes through the rotor disc

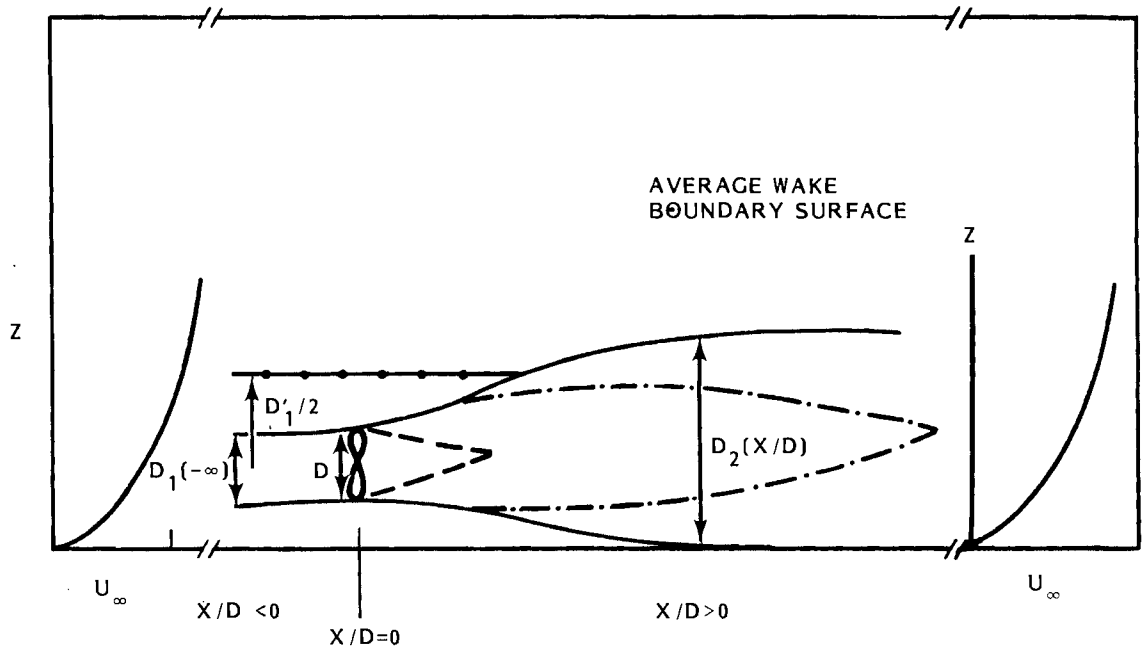

FIGURE 20. Side-view sketch of boundaries of wake and of air flowing into wake. The wind at the right side in the wake has recovered to its left-hand upstream profile. This is indicated by the identical wind profiles graphed on the left and right borders. D_1 is the diameter of the stream tube for upstream that contains all the air that flows through the turbine rotor disc and forms the boundary of the nearest wake. D_1' is the diameter of tube containing air that mixes into wake. D is the diameter of the rotor disc and D_2 is an appropriately defined diameter of the wake at any distance x/D from the rotor.

A' = crosswind area of upstream flow outside A_1 that entrains into the wake in the wake reenergizing process

A_2 = cross axis area of the wake at an arbitrary downwind distance from the turbine

E's = the average energy fluxes through the areas, A, due to fluid transport and/or mixing

$$A_i E_i = \int_{A_i} \frac{d}{dA_i} \frac{d}{dt} \left(\text{energy}_i\right) dA_i \ .$$

P_r = time rate of transfer of energy from the wind to the turbine rotor, the "rotor power".

Equation 1 may be written for simplicity as

$$P_1 + P' = P_r + P_2 \ , \tag{2}$$

where $P_i = A_i E_i$.

The kinetic energy of the airflow may be made up of mean translational wind (P_t), mean wind rotation about the direction of mean translation, or swirl, (P_s) and turbulence fluctuations (P_f). Thus

$$P_1 = P_{1t} + P_{1f} \ . \tag{3}$$

$$P' = P'_t + P'_f \ . \tag{4}$$

$$P_2 = P_{2t} + P_{2f} + P_{2s} \ . \tag{5}$$

The observations presented in previous sections indicate that the turbulence energy change is relatively minor; that is

$$P_{1f} + P_1{}'_f - P_{2f} << P_{1t} + P_1{}'_t - P_r - P_{2t} \ . \tag{6}$$

Similarly the swirl energy is a relatively minor component in the first approximation as measured at x/D = 2. With these minor terms neglected the power balance, Equation (2), becomes

$$P_{1t} + P'_t = P_r + P_{2t} \ . \tag{7}$$

The outer radius of the upwind airflow involved in the wake, D'/2, is to be determined by the value required to produce a balance in Equation (7). We make the further simplifying assumption that the upwind stream tube having diameter D' is circularly symmetric and coaxial with the turbine axis. The energy transport rate of this flow, P_{1t}, may be calculated using the $U_\infty(z)$ profile used in Section 5 and written below as Equation (8).

$$U_\infty = 3.84 \log \frac{(z-z_H+30.5)}{0.05} , \tag{8}$$

where height values are in meters and wind speed is in meters per second.

The energy transport rate in the wake, P_{2t}, is calculated by integrating the energy flux field plotted in Figure 19 over the wake area (enclosed by the dashed line in that figure).

P_r is calculated by the following formula using measured power out of the turbine generator, P_{out}.

$$P_r = \frac{P_{out}}{0.91} . \tag{9}$$

Rearranging Equation (7) and making substitution indicated in Equation (9) we have

$$P'_t = \frac{P_{out}}{0.91} + P_{2t}-P_{1t} . \tag{10}$$

The left-hand term represents the estimated rate of mixing of environmental translational energy into the wake between x/D = 0 and x/D = 2.

An average rate of recovery or reenergizing of the wake for this region may be expressed in nondimensional form as

$$K = \frac{1}{P_{1t}} \frac{dP_2}{d(x/D)} . \tag{11}$$

If we approximate $\frac{dP_2}{d(x/D)}$ by

$$\frac{dP_2}{d(x/D)} \doteq \frac{P_t'}{2-0} , \tag{12}$$

and use (12) and (10) in (11) we have

$$K \doteq \frac{P_{out}}{0.91\ P_{1t}} + \frac{P_{2t}}{P_{1t}} - 1 . \tag{13}$$

Using data presented earlier and area integration of energy flux where appropriate, P_{out} = 192 kW, P_{1t} = 710 kW and P_{2t} = 1207 kW and K = 0.997.

The wake may be considered to have been reenergized when it has mixed with, say, five times the energy flowing through the upstream disc, 5 P_{1t}. If the average rate of energy addition to the wake from x/D = 0 to x/D = 2 were to apply at all distances, a simple integral of power could be formed as follows using Equation (11).

$$\int_{P_{2t}(x/D = 2)}^{P_2(x_e/D)} dP_2 = K \cdot P_{1t} \int_{2}^{(x_e/D)} d(x/D) , \tag{14}$$

where, according to the criteria stated in the paragraph above,

$$P_2(x_e/D) = P_{1t} - \frac{P_{out}}{0.91} + 10 \cdot \frac{P_{out}}{0.91} . \tag{15}$$

Integration of (14) and substitution of (15) into the result gives

$$\frac{x_e}{D} = \frac{5\ P_{1t} - P_{2t}\ (x/D = 2)}{P_{1t} \cdot k} + 2 . \tag{16}$$

Using the numerical values of the quantities in (15) the endpoint of the integration is found to have the magnitude

$$\frac{x_e}{D} = 5.5 \ . \qquad (17)$$

This suggests that the wake could have been negligible at x/D = 5.5.

There is an obvious implication of Equation (17) for spacing of wind turbines in clusters. Its significance is of such importance that we need more new measurements to better describe turbine wakes in real operating conditions. It appears difficult to estimate the rate of recovery of turbine wakes from a few simple wind measurements at one location. Programs for field measurements of wakes often must have less ambitious objectives, such as estimating the following quantities:

1. the approximate width of wake as a function of x/D for a range of values of vertical shear of wind velocity, turbulence energy level and density layering of the atmosphere
2. the approximate centerline velocity deficit as a function of x/D
3. turbulence characteristics of wakes.

8. A COMPARISON OF THE MEASURED WAKE WITH MODELED TURBINE WAKES

Two simple models of a wake are considered, one by Lissaman et al. (1982) and a similar one by Eberle (1981). Both models include turbulent mixing of the wake with the ambient air due to ambient turbulence and to shear-generated turbulence in the edge region of the wake. The following parameters of the wake are compared: 1) the average rate of spread of the wake, 2) the velocity deficit, 3) the vertical and horizontal wind profiles through the nominal center of the wake at x/D = 2, 4) the initial virtual wake diameter, 5) the ratio of horizontal to vertical spread of the wake, and 6) the power ratio for a second identical turbine operating axisymmetrically with the upwind turbine at x/D = 2 from it. The comparisons are made in Table 1 and Figures 21 and 22 based upon values of the parameters selected from the previous sections of this paper and from reports by Eberle and by Lissaman et al.

The vertical profile through the center of the observed wake is plotted along with the inferred upwind profile in Figure 21a using a solid line. The corresponding results from the Eberle model are included on the same graph for downwind distances of x/D = 2.5, 5, 10, 17.5 and 25. The profile observed at x/D = 2 appears to lie in a location that corresponds to a model x/D > 5. Note the vertical offset of the observed vertical profile. This is due to the greater ratio of hub height to rotor radius of the MOD-0A1. The horizontal profiles at hub height are plotted in Figure 21b. Again the observed profile at x/D = 2 appears to correspond to a model profile for x/D > 5. The observed horizontal profile is compared against several model profiles described by Lissaman et al. in Figure 22. The models are adjusted to have the correct centerline velocity deficit and wake width. The general shape of observed profiles is very similar to the model profile shapes.

Considering the simplicity of the models, the rate of spread of the wake is in fair agreement with the observations. Other parameters do not agree well. The wake cross section at x/D = 2 was observed to be far more elliptical

TABLE 1. Comparison of Wake Observation With Several Simple Wake Models

Wake Parameter	Wake Observation Measured on 3 Dec '81	Eberle (1981)	Lissaman et al. (1981)
x/D	2 beyond near wake and transition region	2.5 near wake	3 near wake
σ_u ambient	2 ms^{-1}	---	---
$\sigma_v \equiv 0.6\ \sigma_u$ ambient	1.1 ms^{-1}	---	---
$\frac{\sigma_u}{\bar{U}}$ wake	0.21	---	---
$\frac{\sigma_u}{\bar{U}}$ ambient	0.19	---	---
$\frac{\sigma_v}{\bar{U}}$ ambient	0.10	Pasquill Class D	0.1
Static Stability	neutral	Pasquill Class D neutral	neutral
$X_{POT\ CORE}/D$	< 2	2.5	3
$\bar{U}_\infty$ (z = H)	10.7 ms^{-1}	> 6 ms^{-1}	---
Average spread half angle horiz.	(1% deficit 6.2°) 9.6° 5% profile tail)	6.2°	9.6° (old model)
Average spread half angle vert.	(4° 5% profile tail)	5.9°	14° (new model)
$\frac{\bar{U}_\infty - \bar{U}_e}{\bar{U}_\infty}$	0.26	0.34	0.52
$2R_o/D$ Upstream outer diameter of inflow to wake	energy flux balance method: 1.2	for D/2 = 19.1 m: 1.125	asymptotic stream tube and 1-d momentum theory: 1.5
$\frac{\text{wake horizontal width}}{\text{wake vertical width}}$	1% velocity defect 1.55	computed boundary 1.05	---
a Induction factor	0.13	0.17	0.25
Power Ratio, P/P_∞	0.6	< 0.46	---

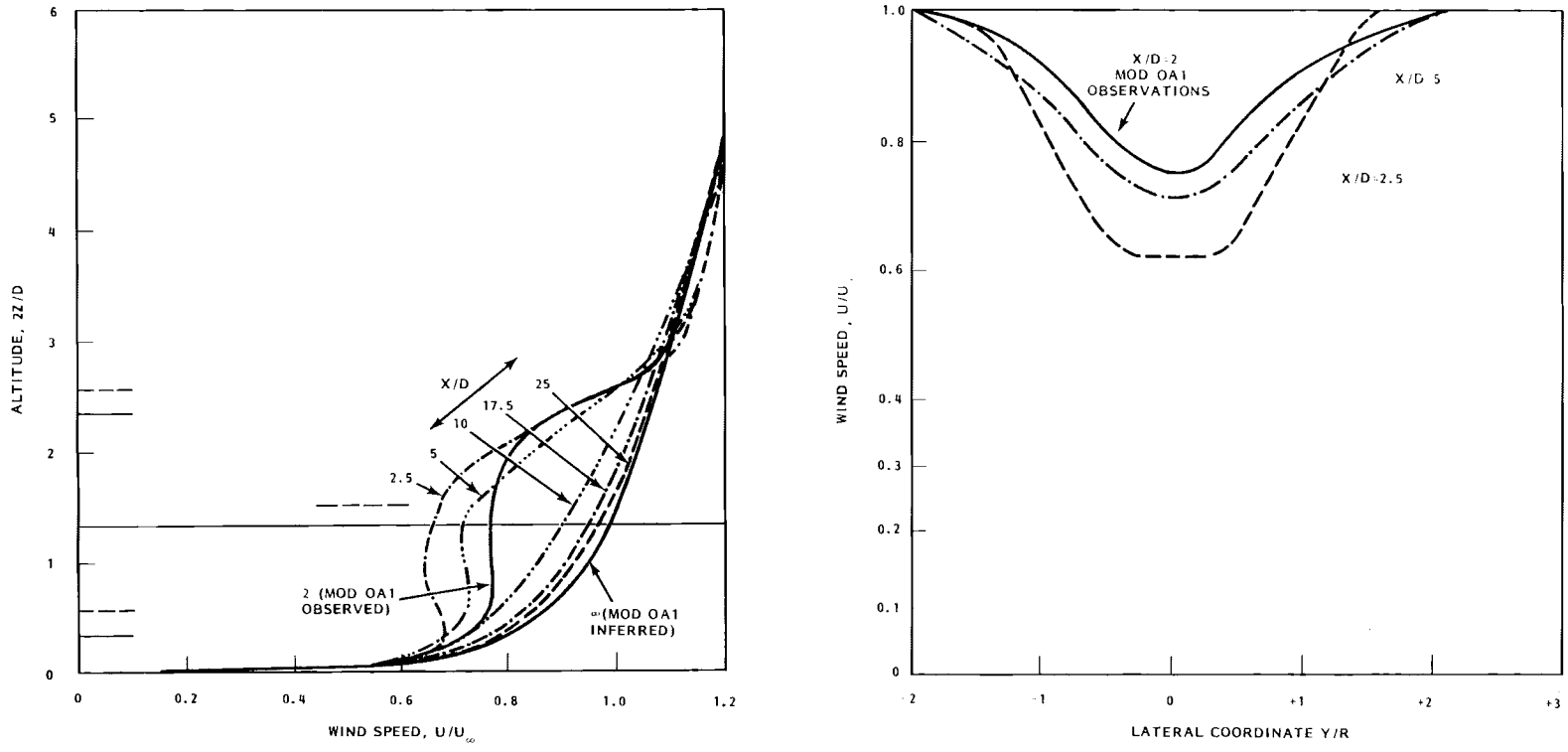

FIGURE 21. A comparison of wake wind speed profiles measured at the VPA and those modeled by Eberle (1981): a) vertical profiles, b) horizontal profiles. The dot-dash lines represent measured profiles. The solid lines represent the model profiles for various values of downwind distance, x/D.

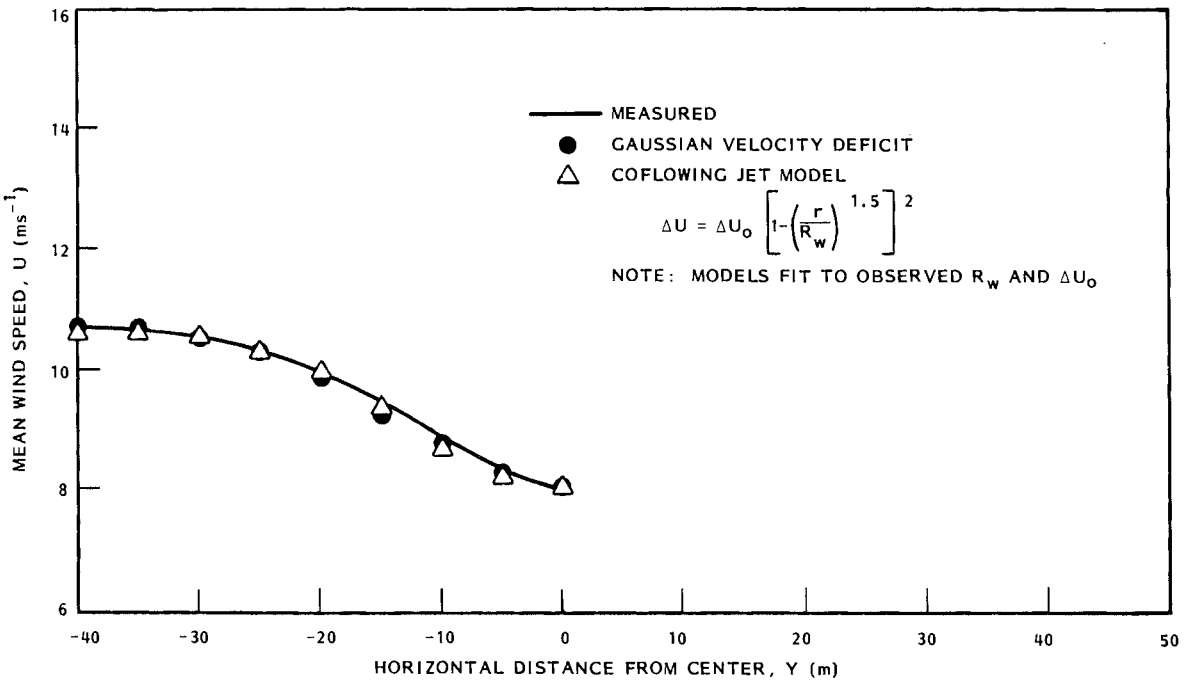

FIGURE 22. Comparison of measured MOD-0A1 wake profile shape with Lissaman wake model profile shapes. Symbols: ● Gaussian velocity deficit model; △ coflowing jet model following Abramovitch. (See Lissaman et al. 1981.) Note: The model profiles are fit to the observed profile by specifying the magnitude of wake width, R_W, and maximum profile deficit, ΔU_o.

than indicated by the models. The simplest statement of the difference between observations and models is that the wake was closer to free stream boundary layer conditions at a much shorter downstream distance than modeled. In the same sense, the observations are in sharp contrast with wakes observed in less turbulent conditions, e.g., the results reported by Hansen (1980) and Vermeulen (1979).

The limited locations of observations do not permit a determination of why the observed wake appears to be a far wake at x/Rd = 2. There are several possibilities. Two are given here:

1. The MOD-0A1 rotor, with a solidity ratio of about 0.04, allows upwind airflow to pass through the rotor disk plane much more freely away from blade location than modeled on a disk-average basis. Thus, a less intense initial wake existed.

2. An interaction between the turbulent fluctuations in the airflow and the rotor blade shed vortices resulted in stronger turbulent mixing than is modeled in the wake region $x < 4$ D.

9. SUMMARY OF OBSERVATIONS

The wake of the MOD-0A1 wind turbine at Clayton, New Mexico has been measured using a vertical plane array of anemometers. The anemometers were in a crosswind plane at a distance of two rotor diameters directly downwind of the turbine. The data were analyzed for a 4.27 minute period when the atmospheric boundary layer and the wake were most stationary. The wind velocities were sampled once every 0.25 second. The following properties of the wake were observed.

Rotor blade vortices were well mixed into the wake turbulence and were not separately detectable at x/D = 2. Wake swirl about the along-wind axis had a value not greater than 0.025 rad s^{-1}. (Note: All wake characteristics described herein are for x/D = 2 unless otherwise stated.) The maximum axial wind speed deficit was $\Delta U/U_\infty = 0.25$.

The axial induction factor, a, calculated using measured winds and one-dimensional momentum theory had a value of a = 0.13 at $U_\infty = 10.7$ ms^{-1}. The NASA aerodynamic model of the MOD-0A1 gave a value of a = 0.13 for $U_\infty = 10$ ms^{-1}.

Extra turbulence energy existed in the edge of the wake at a frequency of about n = 0.025 Hz. This peak of extra turbulence energy existed throughout the wake but diminished toward the center. Spectral peaks at n = 0.25 Hz and 0.50 Hz, equivalent to wavelengths of λ = 1 D and 0.5 D, occurred particularly on the left side of the wake. The wake turbulence integrated over all frequencies is only slightly more energetic than the ambient turbulence. The time integral scale of turbulence in the wake is significantly larger than is expected for the ambient flow.

The cross-wake plane analyses of wind speeds revealed a nearly circular inner portion and a strongly elliptical portion. The elliptical portion major axis was horizontal. The ratio of length of major axis to minor axis had a magnitude of 1.6 based upon the shape of the velocity deficit line for $\Delta U/U_\infty = 0.01$.

An estimate of the average rate of reenergizing of the wake, using measurements of mean wind energy flow and turbine power, suggests that entrainment

with ambient air may have been rapid. The average rate of reenergizing between the turbine and the vertical plane array at x/D = 2 was estimated to be about 700 kW per rotor diameter distance downstream. This is as much energy as flowed through the upstream projection of the rotor disc. If that average rate continued, the wake would be substantially reenergized at a downwind distance of x/D = 5.5. At x/D = 2 the power ratio had a magnitude $P/P_{\infty} = 0.6$.

Some wake characteristics observed on December 3, 1981 were compared with the corresponding ones for several simple wake models (e.g., Lissaman et al. 1982 and Eberle 1981). The models are based upon concepts of mixing of ambient air into a wake or an equivalent coaxial jet. The shapes of the vertical and horizontal profiles of mean wind speed are all very similar. However, the new measurements at x/D = 2 match up with the Eberle model best for $x/D \geq 5$. The rate of spread of the wake was in fair agreement with the models of far wake horizontal spread. Agreement for other properties from theoretical or fluid laboratory simulations was weaker.

Many of the comparisons between the MOD-0A1 wake measurements and the simple models of wakes are made in Table 1.

10. CONCLUDING REMARKS

The observations of a MOD-0A1 wake indicate that the turbine wake entered into a far wake condition close to the turbine on December 3, 1981. The turbine was operating at near rated power and was operating in a neutral-stability atmospheric boundary layer. The microscale wind properties of the wake that affect fatigue and power performance of a second MOD-0A turbine in the wake of the first one suggest that it may be possible for turbines to be successfully operated closer together than was previously thought to be efficient or safe.

Additional modeling and field measurements of wakes are required to improve the understanding of turbine wakes substantially. The complexity of wakes in the atmospheric boundary layer and the difficulty of measuring them has been demonstrated. Useful specializing of wake models for use in turbine and turbine array design may require a few well chosen and well measured wind properties of wakes for each distinctly different type of turbine and location. Wakes in complex terrain will require the greatest skill in measurement and analysis to model accurately the wake conditions that are likely to be found. However, those same airflow complexities may mean that wakes are not as much of a problem for turbines downwind of other turbines in complex terrain.

11. REFERENCES

Blackwell, B. F. and R. E. Sheldahl. 1977. "Selected Wind Tunnel Test Results for the Darrieus Wind Turbine." J. Energy, Vol. 1, No. 6, p. 382.

Boschloo, G. 1977. Wake Structure of a Darrieus Rotor. Netherlands Organization for Applied Scientific Research, TNO Report 77-07244.

Builtjes, P. 1979. Wind Turbine Wake Effects. Netherlands Organization for Applied Scientific Research, TNO Report 79-08375.

Connell, J. R. 1981. The Spectrum of Wind Speed Fluctuations Encountered by a Rotating Blade of Wind Energy Conversion System: Observations and Theory. U.S. DOE, Report No. PNL-4083, 47 pp.

Crafoord, C. 1979. Interaction in Limited Arrays of Windmills. Dept. of Meteorology, Univ. of Stockholm, Report DM-26.

Eberle, W. R. 1981. Wind Flow Characteristics in the Wakes of Large Wind Turbines. Vol. 1 - Analytical Model Development. U.S. Dept. of Energy, Report No. DOE/NASA/0029-1.

Faxen, T. 1979. "Some Meteorological Activities in the National Swedish Wind Energy Program." Proc. Conf. and Workshop on Wind Energy Characteristics and Wind Energy Siting 1979, U.S. DOE and Amer. Meteoro. Soc., 113-130.

Gill, G. C. et al. 1967. "Accuracy of Wind Measurements on Towers or Stacks." Bull. of the Amer. Meteoro. Soc. Vol. 48, No. 9, 665-674.

Hansen, A. C. 1980. Early Results From the SWECS Rotor Wake Measurement Project. Rockwell International Corporation, Energy Systems Group. TM-TD/81-4, 18 pp.

Lissaman, P.B.S. 1979. Energy Effectiveness of Arrays of Wind Energy Collection Systems. Aerovironment, Inc., AVR 6110.

Lissaman, P.B.S. et al. 1982. Numeric Modeling Sensitivity Analyses of the Performance of Wind Turbine Arrays. PNL-4183, Pacific Northwest Laboratory.

Sforza, P. M. et al. 1979. Wind Turbine Generator Wakes. AIAA Paper No. 79-0113, American Institute of Aeronautics and Astronautics.

Vermeulen, P. 1978. A Wind Tunnel Study of the Wake of a Horizontal-Axis Wind Turbine, Netherlands Organization for Applied Scientific Research, TNO Report 78-09674, 19 pp. + Figures and Tables.

Wilson, R. et al. 1976. Aerodynamic Performance of Wind Turbines. Oregon State University, Report unnumbered.

DISTRIBUTION

No. of Copies

OFFSITE

C. I. Aspliden
Battelle Memorial Institute
Washington Operations Office
2030 M Street, N.W.
Washington, DC 20036

D. F. Ancona
Department of Energy
Wind Energy Technology Division
1000 Independence Avenue
Forrestal Building, Room 5F059
Washington, DC 20585

S. D. Berwager
Department of Energy
Wind Energy Technology Division
1000 Independence Avenue, S. W.
Forrestal Building, Room 5F059
Washington, DC 20585

Jack Cadogan
Wind Energy Technology Division
Forrestal Building, Room 5F059
1000 Independence Avenue, S. W.
Washington, DC 20585

L. V. Divone
Department of Energy
Wind Energy Technology Division
1000 Independence Avenue
Forrestal Building, Room 5F059
Washington, DC 20585

W. C. Reddick
Department of Energy
Wind Energy Technology Division
1000 Independence Avenue
Forrestal Building
Washington, DC 20585

No. of Copies

G. P. Tennyson
Department of Energy
Albuquerque Operations Office
P.O. Box 5400
Albuquerque, NM 87115

27 DOE Technical Information Center

2 Tom Zambrano/Graham Gyatt
Aerovironment, Inc.
143 North Vista Avenue
Pasadena, CA 91107

Clarissa Quinlan
Alaska State Energy Office
338 Denali Street
Anchorage, AK 99501

D. K. Ai
Alcoa Laboratories
Alcoa Technical Center
Alcoa Center, PA 15069

Tom Gray
American Wind Energy Association
1621 Connecticut Avenue, N.W.
Washington, DC 20009

Richard Katzenberg
American Wind Energy Association
Natural Power, Inc.
New Boston, NH 03070

A. B. Van Rennes
The Bendix Corporation
Executive Offices
Bendix Center
Southfield, MI 48037

No. of Copies

John Lowe
Boeing Engineering and Construction
P.O. Box 3707
Mail Stop 9A-65
Seattle, WA 98124

Don Nielson
Boeing Engineering and
Construction Co.
P.O. Box 3707, MS-9A-65
Seattle, WA 98124

Nick Butler/Ron Holman
Bonneville Power Administration
P.O. Box 3621
Portland, OR 97208

S. J. Hightower
Bureau of Reclamation
Denver Federal Center
Building 67, Code 254
Denver, CO 80225

Joe Hennessy
Wind Energy Program
California Energy Commission
1111 Howe Avenue, Mail Stop 66
Sacramento, CA 95825

Tom Hoffer
Desert Research Institute
Atmospheric Sciences Center
University of Nevada System
P.O. Box 60220
Reno, NV 89506

J. Telford
Desert Research Institute
Atmospheric Sciences Center
University of Nevada System
P.O. Box 60220
Reno, NV 89506

No. of Copies

Edgar DeMeo
Electric Power Research Institute
3412 Hillview Avenue
Palo Alto, CA 94303

Walter Frost
FWG Associates, Inc.
271A Lakewood Drive
Tullahoma, TN 37388

George Fichtl
7703 Oakridge Drive
Huntsville, AL 35802

2 Tom Hiester/Dr. Peter Liu
Flow Industries, Inc.
21414-68th Avenue South
Kent, WA 98031

Daniel DiGiovacchino
Advanced Energy Programs Department
General Electric Company
501 Allendale Road, P.O. Box 527
King of Prussia, PA 19406

Stanley Macklis
General Electric Company
Advanced Energy Systems
P.O. Box 8661
Philadelphia, PA 19101

J. M. Kos
Hamilton Standard
Bradley Field Road
Windsor Locks, CT 06096

Jean Mayhew
Hamilton Standard, MS-IM3
Bradley Field Road
Windsor Locks, CT 06095

M. A. Bowes
Kaman Aerospace Corporation
Old Windsor Road
Bloomfield, CT 06095

No. of Copies

W. A. Vashon
A. D. Little, Inc.
20 Acorn Park
Cambridge, MA 02140

Abbey Page
Maine Office of Energy Resources
55 Capital
Augusta, ME 04330

J. Konigsberg
Montana Energy Office
Capital Station
Helena, MT 59601

Darryl Baldwin
NASA/Lewis Research Center
21000 Brookpark Road
Cleveland, OH 44135

Dave Spera
NASA/Lewis Research Center
21000 Brookpark Road
Cleveland, OH 44135

J. C. Kaimal
National Oceanic & Atmospheric
Administration/Wave Propagation
Laboratory
3000 Marine Street
Boulder, CO 80302

W. Holley
Department of Mechanical Engineering
Oregon State University
Corvallis, OR 97331

R. Thresher
Department of Mechanical Engineering
Oregon State University
Corvallis, OR 97331

J. E. Wade/Bob Baker
Department of Atmospheric Sciences
Oregon State University
Corvallis, OR 97331

No. of Copies

J. Dutton
Department of Meteorology
Pennsylvania State University
University Park, PA 16902

H. A. Panofsky
Department of Meteorology
Pennsylvania State University
University Park, PA 16902

A. C. Hansen
Rockwell International
P.O. Box 464
Golden, CO 80401

R. Akins
Sandia Labs 4715
Box 5800
Albuquerque, NM 87165

E. G. Kadlec
Sandia Labs 4715
Box 5800
Albuquerque, NM 87165

Rick Mitchell
Solar Energy Research Institute
1617 Cole Boulevard
Golden, CO 80401

Robert Scheffler
Southern California Edison
P.O. Box 800
Rosemead, CA 91770

Don Bain
Department of Energy
State of Oregon
Labor and Industries Building
Room 111
Salem, OR 98310

Dr. Chip Meserole
U.S. Windpower, Inc.
160 Wheeler Road
Burlington, MA 01803

No. of Copies

R. H. Kirchhoff
Department of Mechanical Engineering
University of Massachusetts
Amherst, MA 01003

Dean Harwell
University of Tennessee Space Institute
Tullahoma, TN 37388

H. Tielman
Department of Engineering Sciences & Mechanics
Virginia Polytechnic and State University
Blacksburg, VA 24061

Susan Hosch
Washington State Energy Office
400 E. Union Avenue, 1st Floor
Olympia, WA 98504

T. Anderson
Westinghouse Electric Co.
P.O. Box 10824
Pittsburgh, PA 15236

Ron Nierenberg
Windfarms, Ltd.
639 Front Street
San Francisco, CA 94111

Dr. V. Barros
28 De Julio 28
9120 Puerto Madryn
Chulret
R. ARGENTINA

D. Lindley
Taylor Woodrow Construction, Ltd.
Taywood House
345 Ruislip Road
Southall
Middlesex UBI 2QX
ENGLAND

No. of Copies

D. T. Swift-Hook, Head
Applied Physics Division
Central Electricity Research Laboratories
Kelvin Avenue
Leatherhead
Surrey
KT 22 7SE
ENGLAND

Dr. Neil Cherry
Lincoln College
Canterbury
NEW ZEALAND

ONSITE

1 DOE Richland Operations Office

H. E. Ransom

37 Pacific Northwest Laboratory

D. B. Cearlock
W. C. Cliff
J. R. Connell
J. C. Doran
C. E. Elderkin
R. L. George
A. H. Miller
E. L. Owczarski
D. C. Powell
J. V. Ramsdell
D. S. Renné
H. L. Wegley
L. L. Wendell
R. K. Woodruff
Technical Information (5)
Publishing Coordination (2)
WCPE Program Office (15)
2400 Stevens Library